Signal Propagation in Neuron And Its Dynamical Behavior

by

Sudipta Ray

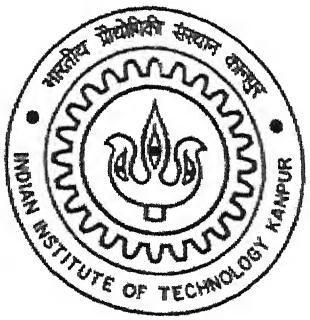

DEPARTMENT OF ELECTRICAL ENGINEERING

Indian Institute of Technology Kanpur

June 2005

Signal Propagation in Neuron And Its Dynamical Behavior

A Thesis Submitted

in Partial Fulfillment of the Requirements

for the Degree of

Master of Technology

by

Sudipta Ray

to the

DEPARTMENT OF ELECTRICAL ENGINEERING

Indian Institute of Technology Kanpur

June 2005

CERTIFICATE

It is certified that the work contained in the thesis entitled "*Signal Propagation in Neuron And Its Dynamical Behavior*" by *Sudipta Ray* has been carried out under my supervision and that this work has not been submitted elsewhere for a degree.

(Prem K. Kalra)

June 2005

Professor,

Department of Electrical Engineering,

Indian Institute of Technology Kanpur,

KANPUR - 208 016 (INDIA)

Dedicated to

My parents whose un-repayable love

always inspires me.

Acknowledgments

A journey is easier when you travel together. Interdependence is certainly more valuable than independence. During the last two years, I have come across many people who helped and accompanied me on the path of completing this thesis successfully. I sincerely thank all of them. Among my well wishers, I express gratitude from the soul of mine to my thesis supervisor Prof. Prem K. Kalra who not only acted as my guide, but also as a guardian during my stay at IIT Kanpur. I feel fortunate to work under him.

I am immensely thankful to Khullar Sir, R.N. Yadav, K. V. Arya, Abhishek Yadav, Deepak Mishra, Vrijendra Singh, and Tukaram Moger who advised and supported me whenever needed. I would also like to thank Deepti Pathak, Gurpreet Singh, Md. Shiblee, Ashutosh Dwivedi, Nimit Kumar, Sandeep Yadav, Anu Verma, Ajay Kiran, B. K. Tripathi, Yogesh Bichpuria, and Surkhan Singh for making the working environment of the lab a friendly one.

I am auspicious to enjoy the company of my friends Kingshuk Kr. Das, Abhishek Agrawal, Prabodh Dewangan, Mahesh Kr. Reddy, Telari Manojaya, Antara Digar, Sutapa Hazra, Trishikhi Raychoudhuri, Shahana Chatterjee, Pavan Shukla, Swapnil Shukla, Amit Singhai, K. Jayalakshmi, V. Siddharth, and G. Shrikanth with whom I spent memorable times during the last two years. I thank my friends Achintya Banerjee, Suman Banerjee, Mrinmoy Nag, Pritam Dutta, B. Shashikant, Eldo Zacharia, Tantanu Mishra, Somnath Bhattacharya, Anirban Roychoudhuri, Sujith S., Diwan

Singh Yadav, Lakshmi Narasimha, Nandakumaran R., Kasiraj Sri Harsha, Urmila Prakash, Priya Ravindranath, Shilpa M. V., Subhrangshu Sen, Avishek Biswas, Suman Sarkar, Anindya Kundu, Rajesh Dubey, and Doel Sengupta who accompanied me since a very early stage of life.

Sudipta Ray

ABSTRACT

The neurons work together to process the information in nervous system that in turn controls the animal behaviors. This is an attempt to understand the dynamics of one of the basic components of central nervous system *i.e.*, neuron. Exploring the dynamical characteristics of neuron is very helpful in uncovering the mechanism behind brain functions. Along with this, revealing the parallel processing in brain requires knowledge of coupling and synchronization among different neurons. In this thesis work, the dynamical features and effect of coupling strengths on synchronization in network of neurons are studied. Bifurcation analysis are carried out to find out the variation in excitability considering stimulus intensity as the bifurcation parameter. Besides the dynamics of point neuron, the signal propagation in the neuron structure is also investigated. The neuron structure consists of amalgamation of dendrites, soma, axon and synapse each exhibiting different dynamics. The study of signal propagation in complete neuron structure is helpful to depict the dynamics of biophysical activities. The effect of random opening and closing of ion gates and ephaptic interaction are taken care of by adding white Gaussian noise in the analysis. A different method to evaluate signal propagation is proposed which is based on calculation of Fourier coefficients from the generated wave.

Notations

Notation	Description	Dimension
t	Time	ms
τ	Time Constant	ms
x	Distance	$mm,\ cm$
V_m	Membrane Potential, Action Potential	mV
V_{Rest}	Resting Membrane Potential	mV
$R,\ R_m$	Membrane Resistance	$K\Omega - cm^2$
G_M	Membrane Conductance	mS/cm^2
I_{inj}	Stimulus	nA
k_B	Boltzmann constant	$m^2Kg/(s^2K)$
T	Absolute Temperature	K
q	Charge of a single Proton	C
$\overline{G}_{channel}$	Maximum conductance of an Ion Channel	mS/cm^2
$g_{channel}$	Conductance of an Ion Channel	mS/cm^2
z	Valence of Ion	
$[B]$	Concentration of B ions	mM
p_a	Activation Variable	
p_{da}	Deactivation Variable	

Notation	Description	Dimension
ζ_a	Number of Activation Channel	
ζ_{da}	Number of Deactivation Channel	
$\overline{G}_{Na}$	Maximum Conductance of Sodium Channel	mS/cm^2
$\overline{G}_K$	Maximum Conductance of Potassium Channel	mS/cm^2
$\overline{G}_{Ca}$	Maximum Conductance of Calcium Channel	mS/cm^2
G_L	Leakage Conductance	mS/cm^2
g_{Na}	Conductance of Sodium Channel	mS/cm^2
g_K	Conductance of Potassium Channel	mS/cm^2
g_{Ca}	Conductance of Calcium Channel	mS/cm^2
m	Activation Variable for Sodium Channel	
h	Deactivation Variable for Sodium Channel	
$n,\ w$	Activation Variable for Potassium Channel	
m_∞	Steady state Calcium Activation	
w_∞	Steady state Potassium Activation	
τ_w	Time Constant for Morris-Lecar Model	
α_x	Rate Constant: Transition from closed to open state	s^{-1}
β_x	Rate Constant: Transition from open to closed state	s^{-1}
E_L	Equilibrium Leakage Potential	mV
E_{Na}	Equilibrium Sodium Potential	mV
E_K	Equilibrium Potassium Potenti	mV
E_{Ca}	Equilibrium Calcium Potential	mV
E_{syn}	Synaptic Potential	mV
g_{syn}	Synaptic Conductance	mS/cm^2
t_{peak}	Time to reach peak value for NMDA Current	ms

Notation	Description	Dimension
$\tau_1,\ \tau_2$	Time Constants: Non-NMDA Synapse	ms
$g_c^{i,j}$	Coupling Conductance between two Neurons	mS/cm^2
ψ^*	Equilibrium point value of any Variable ψ	Same as ψ
J	Jacobian	
λ	Eigenvalue	
r_L	Intracellular Resistivity	$K\Omega - mm$
i_m	Membrane Current	nA
a	Radius of Cable	μm
ξ	Space Constant	mm
R_ξ	Longitudinal Resistance	$K\Omega$
μ	Compartment Number	
$g^{\mu,\mu'}$	Coupling Conductance between two Compartments	mS/cm^2
η	White Gaussian Noise	dBW
$a_k,\ b_k$	Fourier Coefficients	
c	Speed of Wave	cm/ms
VD	Potential of Dendrite	mV
K	Constant	mS
RD	Coupling Resistance between Soma and Dendrite	$K\Omega$
R_S	Soma Resistance	$K\Omega$
V_S	Summed Potential at Soma	mV

Contents

List of Figures

Chapter 1

Introduction

The study of dynamical behavior of the nervous system has drawn huge attention during the last few decades. The main aim of this study is to find out the functioning of brain. Despite a lot of attempts, the proper mechanism of the brain is still unclear. The smallest integral part of any nervous system is neuron. Exploring the behavior of neuron will be very helpful to uncover the details of the brain dynamics. Brain dynamics include information processing in neurons such as generation of spike, its propagation, communication among neurons, bifurcation analysis, presence of chaos, synchronous behavior etc. In this thesis, effort is made to analyze the synchronous behavior of neuron and information transmission in nerve cells by applying nonlinear dynamical analysis techniques.

1.1 Motivation

The brain allows the synchronous functioning of neurons so that the neuronal system work more efficiently. Present trends of research include investigation of the behavior of neurons when considered in a network. Researchers have concentrated their study mainly on the dynamics of two coupled neurons. The extension of this study on increased number of neurons may yield significant results. Also, the studies have been

carried out on different parts of neurons *viz.* dendrites, soma and axon separately which helps in knowing the flow of information from one end to the other. The response for complete neuron structure is required in order to understand the phenomena occurring in small networks of nervous system. A better approach to model the signal propagation is needed that would be easier to compute when compared to previous methods.

1.2 Literature Survey

The simplest model of the nervous system is given by the dynamics of a point neuron. The first attempt to predict the neuronal behavior was given by Lapicque in 1907 [22]. He modeled the membrane as an RC circuit and introduced a spike artificially if the membrane potential crosses a threshold value. The model is known as *Integrate-and-Fire* model. The effect of ion channels are not considered in this model. In 1952, Hodgkin and Huxley proposed a biophysical model of the active membrane that incorporates the dynamics of ion channels [17]. *Hodgkin-Huxley* model considers the membrane current as a composition of leakage current, sodium current and potassium current. This model is four dimensional and hence complex and computationally inefficient. FitzHugh [12] proposed a simplified version of the Hodgkin-Huxley model. Nagumo *et. al.* derived the equations those qualitatively describe the events occurring in an excitable neuron [27]. The models proposed by them are combined together to give a two dimensional model known as *FitzHugh-Nagumo* model. This model replicates the biophysical activities in terms of fast and slow variables. FitzHugh-Nagumo neuronal model is very simple and widely used by different researchers to understand the brain phenomena. Because this model does not represent any physical membrane, Morris and Lecar proposed a two dimensional model that portraits the dynamics of barnacle muscle fiber [25]. This model, known as *Morris-Lecar* model, considers the effect of calcium channel. It has many variants depending upon its parameter value, the values given by Rinzel [35] are widely used for analysis. All these models represent

either *Type-I* or *Type-II* membrane classified based on their firing frequency. A variant of neurons also exhibits the bursting phenomenon that is not captured by these popular neuron models. Rinzel proposed a modified three dimensional version [33] of FitzHugh-Ngumo model known as *FitzHugh-Rinzel* or *Modified FitzHugh-Nagumo* model. It shows the bursting in neurons.

For parallel processing in brain, the neurons must synchronize with each other. The synchronization allows efficient execution of any task. There have been physical evidences of coupling in nervous systems. A study of coupling in the developing mammalian retina has been carried out by Penn [28]. Gerloff *et. al.* showed that task-related coherence reflects inter-regional functional coupling of oscillatory neuronal activity [14]. The recent trends in computational neuroscience research is to study the synchronizing behavior among neurons. An experimental study on a pair of biological neuron that interact through naturally occurring electrical coupling shows that the natural coupling synchronizes slow oscillations of membrane potentials [10]. Ucar *et. al.* have studied the effect of coupling in FitzHugh-Nagumo system and designed an active controller that synchronizes the weakly coupled neurons [42].

The local neural dynamics is determined by voltage-and ligand-gated ion channels and feedback between densely interconnected excitatory and inhibitory neurons. With modulation of long-range synaptic coupling, the system undergoes a transition from independent oscillations to stable chaotic synchronization [4]. Bifurcation analysis predicts the effect of parameter variation in any dynamical systems [38]. Rinzel and Ermentrout studied the bifurcations in the Morris-Lecar model by treating the externally applied dc current as bifurcation parameter [34]. A bifurcation analysis and investigation of presence of chaos is studied in [13], [19] and [24]. Like single neuron models, the bifurcation analysis on coupled neuron models also reveals significant informations. In [2], a study is carried out in excitable chaos in coupled FitzHugh-Nagumo model. Kavasseri has investigated bifurcations in synaptically coupled Morris-Lecar model [21]. Similar to chaos and bifurcation, the study of noise is also important in nervous systems

as there are many sources of noise such as *Synaptic bombardment*, *Ephaptic Interaction* and uneven opening and closing of ion channels. Noise may change the behavior of the system drastically. The stochastic resonance helps in signal detection of neurons [37]. Tuckwell and Rodriguez showed both analytical and simulation results for stochastic FitzHugh-Nagumo model [41]. The authors in [32] carried out a similar analysis on Hindmarsh-Rose model.

All of these studies have been carried out on point neuron models. However, there is a need to carry out analysis on axon and dendritic tree. The neuronal spikes show different characteristics when they travel along active axon or passive dendritic trees. There is a delay as well as decay in spike when it propagates through passive membrane [9]. The delay depends upon the speed of the spike which in turn depends on the topology of the cable. The speed of action potential in a giant axon of squid is 18.8 m/s [26]. The axon stem branches out near soma. This results in a change of speed. The diameters of the daughter branches do follow a pattern. A method to find out these diameters is given in [6]. The ion channels embedded in axon helps in proper propagation of action potential. The range of ion concentration that should be present for a successful propagation of signal is studied in [43]. Gordon and Welsh [15] discussed about ion channels embedded in axon. The axons of different neurons dissipate a certain energy to produce a spike. Authors in [3] studied the energy requirement for spike propagation. The *Ephaptic Interaction* [18] depolarizes the axon and thus helps in signal propagation. This interaction occurs between two axons closely located and touching each other. The interaction between nerve fibers are also studied in [7] and [16]. Arvanitaki suggested that *Ephaptic Interactions* presume electrical fields in extracellular space generated by active neurons induce current flow in adjacent neurons [1]. There may be generation of spike in the dendrites if it is spine studded. An analysis supporting this phenomenon has been carried out by Coombes and Lord [23]. The traveling waves in dendrites may also be periodic [8]. The periodic response in axonal propagation has been found by Terakawa [40]

1.3 Organization

The thesis work has been organized in four chapters.

Chapter 2 discusses on neuron and its dynamical behaviors. It presents a brief introduction on neuron structures and describes its characteristics. The dynamics of active and passive membranes and that of synapse has been studied. The effect of coupling on neuronal behavior is found out by investigating the synchronizing conditions and bifurcation analysis.

Chapter 3 covers the studies on the signal propagation in neuron. It focuses the important aspects of the models for signal propagation in dendrites and axon. Effect of noise on axon has been examined. A new method based on *Fourier series* has been proposed to model the axon. Finally, the picture of signal propagation and neuronal communication have been portrayed with the help of complete neuron structure.

Chapter 4 gives the conclusions based on findings and suggests some future scopes.

Chapter 2

Neuron and Its Dynamics

2.1 Structure of Neuron

The information processing in nervous system is perhaps the most existing complex phenomenon in the world. The basic building block of the nervous system is neuron. According to biologists, a human brain consists of approximately 100 billion neurons with each neuron having at least 10,000 connections with other neurons. The communication between two neurons usually takes place through synapse, a gap separating two neighboring neurons. Sometimes the neuron communicates through *Ephaptic Transmission* which is nonsynaptic electrical interaction[22]. The neurons are similar to the other cells in the bodies [46] as

- Neurons are surrounded by a cell membrane
- Neurons have a nucleus that contains genes.
- Neurons contain cytoplasm, mitochondria and other organelles
- Neurons carry out basic cellular processes such as protein synthesis and energy production.

On the other hand, neurons have some properties that distinguish it from other cells and these properties are

- Neurons have specialized extensions called dendrites and axons. Dendrites bring information to the cell body and axons take information away from the cell body.
- Neurons communicate with each other through an electrochemical process.
- Neurons contain some specialized structures *eg.* synapse and chemicals *eg.* neurotransmitters.

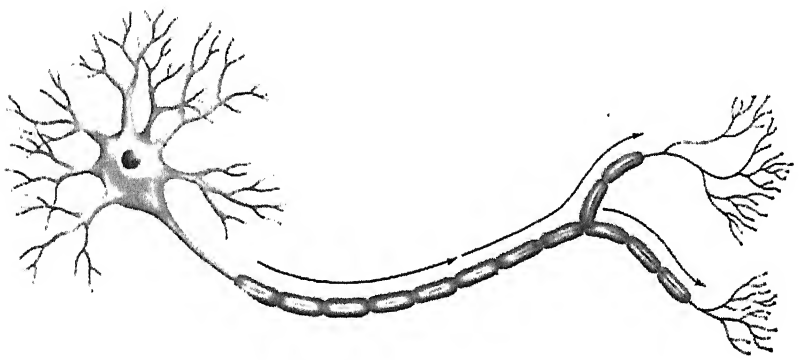

Figure 2.1: Architecture of a neuron

A neuron has three major morphologically defined portions: soma, dendrite and axon [20]. Each of these parts makes a specific contribution to the processing of nerve signals. Figure 2.1 [1] shows the structure of a typical neuron found in vertebrates. The soma also known as cell body consists of the cell nucleus and perikaryon. It is usually 50 μm or more in diameter. The dendrites branch out from soma in treelike fashion. These are short nerve fibers and highly branched. The dendrites exist in many per cell

[1] Figure 2.1is taken from [47]

and covers approximately $80-90\%$ of the total surface area of neuron. Axon is slender and may be very long. It has a diameter ranging from 0.2 to 20 μm and a length up to $1m$. It has several branches at its end near synapse. Sometimes, the axon is covered with myelin sheath consists of fat-containing cells that insulate the axon. The gaps (approximately 1 μm wide) formed between myelin sheath cells long the axons are called *Nodes of Ranvier*. A neuron has only one axon. It begins at the *Axon hillock*. The dendrites recieve inputs from the axon terminal of other neurons at synapse. The electrical signals travel along the dendrites to soma and aggregation takes place there. The summed signal travels down the axon to synapse where it stimulates the dendrites of other neurons. The myelin sheath allows rapid and efficient transmission of impulses along the nerve cells.

Cell morphology may be classified according to the number of elements emanating from the cell body [36] as unipolar cells, bipolar cells and multipolar cells. The unipolar cells are generally found in invertebrates while multipolar cells are dominant in vertebrate nervous systems. Neurons can be further classified by the direction that they send information:

- Sensory or afferent neurons that send information from sensory receptors *viz.* eyes, ears, nose, tongue and skin toward the central nervous system.
- Motor or efferent neurons send information away from the central nervous system to muscle or glands.
- Interneurons send information between sensory neurons and motor neurons.

Each type of neuron poses different characteristics. The neurons are mainly classified as *Type-I*, *Type-II*, and *Type-III* based on their dynamical response. Among these, the dynamics of *Type-I* and *Type-II* neuron models have been considered for the study as the most of the neurons follow either of the two characteristics.

2.2 Neuron Modeling

2.2.1 Membrane Equation

The cell membrane is a lipid bilayer, usually $3-4\ nm$ thick, that is essentially impermeable to most charged molecules. A cubic micron of cytoplasm might contain 10^{10} water molecules, 10^8 ions, 10^7 small molecules and 10^5 proteins [9]. The mobility and repelling nature of the ions and the molecules that carry charges may result in a build up of negative charges inside the membrane. Electrostatic forces attract an equal density of positive ions from the extracellular medium to the outside surface of the membrane. The insulating nature causes the membrane to act like a capacitor by separating the charges lying along its interior and exterior surface. Numerous ion channels are embedded in the cell membrane. The ion channels are highly selective in most of the cases allowing only a single type of ion to pass through them. These ion channels eventually lower the effective membrane resistance to a value about 10000 times smaller than that of a pure lipid bilayer. When the neuron is inactive, the excess internal negative charges cause the potential inside the cell membrane to be negative. This potential is known as *Resting Potential* and denoted by V_{Rest}.

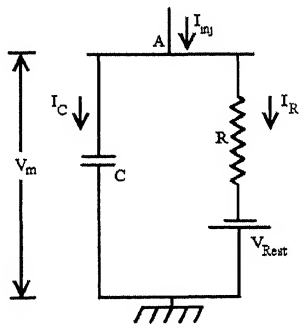

Figure 2.2: Circuit representation of a passive membrane

Thus a membrane can be represented in most simple way by a parallel combination

of a capacitance with a series connection between a resistor and a battery as shown in Figure 2.2. The dynamics of this linear model can be found out by applying KCL at node A. It results in Equation 2.1

$$\tau \frac{dV_m(t)}{dt} = -V_m(t) + V_{Rest} + RI_{inj}(t) \tag{2.1}$$

Where $\tau = RC$. The solution of Equation 2.1 for a step current input with magnitude I_0 is given by Equation 2.2

$$V_m(t) = RI_0 \left(1 - e^{-t/\tau}\right) + V_{Rest} \tag{2.2}$$

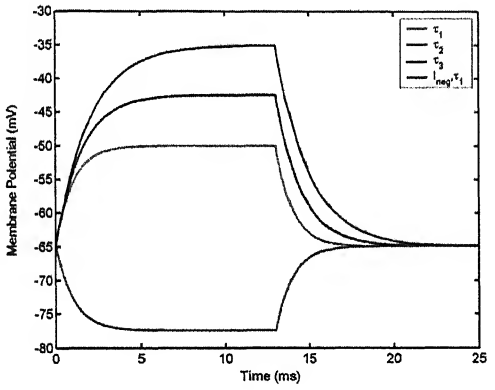

Figure 2.3: Response of passive membrane

If the current injection is stopped at time t_{off} after the membrane potential reaches the steady state value, then the membrane potential returns to V_{Rest} with an exponential time course given by,

$$V_m(t) = RI_0 \, e^{-(t-t_{off})/\tau} + V_{Rest} \tag{2.3}$$

The response of the passive membrane modeled using a simple R-C circuit is shown in Figure 2.3. The red, blue and black lines correspond to membrane potential at different time constants τ_1, τ_1, and τ_3 respectively with $\tau_3 > \tau_2 > \tau_1$. The magnitude of injected

current is same for all the cases. It has been verified that, the membrane potential reaches its steady state value more rapidly for lower values of time constant. For lower values of time constants, the passive membrane of dendrites reacts to a synaptic current change more rapidly. The green line shows the response of the membrane potential with the time constant value τ_1 and subjected under inhibitory current. As depicted from Figure 2.3, the dynamics of passive membrane represents the subthreshold region.

2.2.2 Point Neuron Models

The first attempt to represent the neuronal activities in terms of mathematical equations was formulated in 1907 by Lapicque. Different mathematical models have been developed later on to represent the biological activities in a more detailed manner. Out of these models, the models that are found more frequently in literature are Leaky Integrate and Fire (LIF) [22], Hodgkin-Huxley (HH) [17], FitzHugh-Nagumo (FHN) [12], [27] and Morris-Lecar (ML) [25] neuron model. The HH, FHN and ML models consider the dynamics of different ion gates. These ion gates are highly selective and usually allow only a single type of ion to pass through it. Each of these channels may be represented as a battery in series with nonlinear voltage dependent conductance as shown in Figure 2.4. The potential offered by the membrane may be found out through *Nernst Equation* given in Equation 2.4.

$$E = \frac{V_T}{z} \ln \left(\frac{[ion(outside)]}{[ion(inside)]} \right) \tag{2.4}$$

where z is the valence of ion and V_T is typical membrane potential. It has a value between 24 mV to 27 mV for the typical temperatures of cold and warm blooded animals [9]. The membrane potential varies from -3 to $+2$ times of V_T.

The expression for typical membrane potential is given by Equation 2.5

$$V_T = \frac{k_B T}{q} \tag{2.5}$$

where k_B is the *Boltzman constant*, T is absolute temperature, and q is charge of a single proton.

The channel conductance are given by the following expressions.

$$g_{channel}(V_m) = \overline{G}_{channel}\left(p_a^{\zeta_a} p_{da}^{\zeta_{da}}\right) \tag{2.6}$$

where the channel has ζ_a activation and ζ_{da} deactivation ion gates. p_a and p_{da} represents the probability that the corresponding type of ion gate is open at any time instant. These ion gates are voltage dependent and hence vary with any change in membrane potential. $\overline{G}_{channel}$ is the maximum possible conductance of the channel.

Among the above mentioned models, the HH neuron model represents the dynamics of *Type-II* and ML model represents the same of *Type-I* neuron model. Therefore these two models are considered for analysis to cover up the different types of behavior observed in a neuron.

2.2.3 Hodgkin-Huxley Model

Hodgkin and Huxley proposed a neuron model [17] from the experimental data obtained by artificially stimulating the giant axon of squid. This model considers only the dynamics of sodium and potassium ion channels *i.e.* only these two channels are assumed to pose voltage dependent nonlinear conductance. Other ion channels are assumed to follow *Ohm's Law*. The potassium channel is comprises of four activation gates whose opening probability is assumed to be n. The sodium channel has three activation gates with opening probability of m and a single deactivation gate with opening probability h. The circuit diagram of the model is shown in Figure 2.4. The dynamics of the model is given in Equation 2.7.

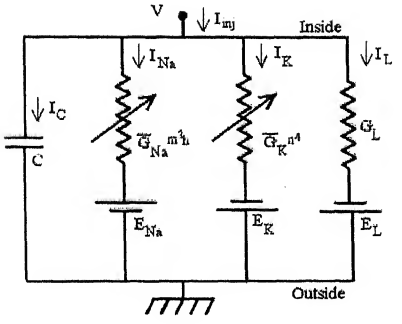

Figure 2.4: Circuit representation of Hodgkin-Huxley model

$$C\frac{dV_m(t)}{dt} = \overline{G}_{Na}m^3h\left(E_{Na} - V_m(t)\right) + \overline{G}_K n^4\left(E_K - V_m(t)\right) + G_L\left(E_L - V_m\right) + I_{inj}(t) \tag{2.7}$$

$$\frac{ds(t)}{dt} = \alpha_s(V_m)\left(1 - s(t)\right) - \beta_s(V_m)s(t); \quad s \in n, m, h$$

$\alpha_s(V_m)$ and $\beta_s(V_m)$ are voltage dependent rate constants. $\alpha_s(V_m)$ determines the number of transitions that occur from the closed to open states and $\beta_s(V_m)$ specifies the same from the open to closed states. These rate constants for the variables n, m, and h can be expressed as

$$\alpha_n(V_m) = \frac{10 - V_m}{100\left(e^{(10-V_m)/10} - 1\right)}; \qquad \beta_n(V_m) = 0.125\ e^{-V_m/80}$$

$$\alpha_m(V_m) = \frac{25 - V_m}{10\left(e^{(25-V_m)/10} - 1\right)}; \qquad \beta_m(V_m) = 4\ e^{-V_m/18}$$

$$\alpha_h(V_m) = 0.07\ e^{-V_m/20}; \qquad \beta_h(V_m) = \frac{1}{e^{(30-V_m)/10} + 1}$$

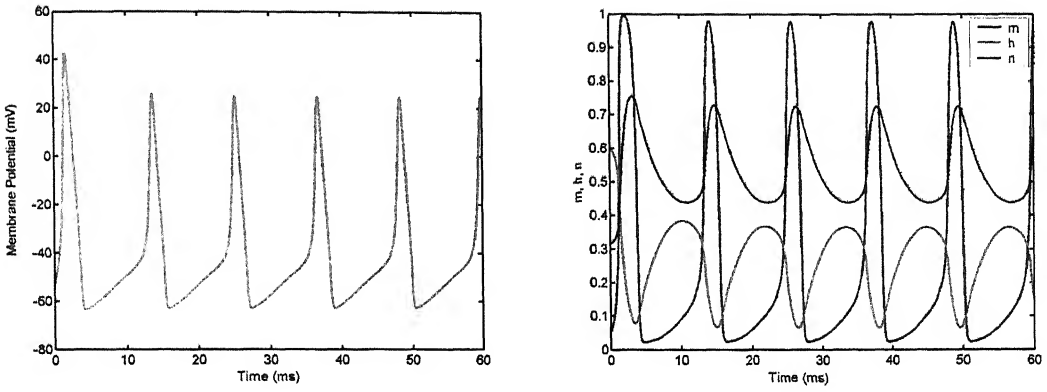

(a) Membrane potential (b) Time course of gating variables

Figure 2.5: Response of Hodgkin-Huxley model

The parameter values of HH model for a typical membrane are $\overline{G}_{Na} = 120\ mS/cm^2$, $E_{Na} = 115\ mV$, $\overline{G}_K = 36\ mS/cm^2$, $E_K = -12\ mV, G_L = 0.3\ mS/cm^2$, $E_L = 0\ mV$ [22]. Potential parameter values considered are taken with respect to the resting potential of membrane. Response of the model is plotted in Figure 2.5. Part (a) shows the variation of membrane potential with respect to time. The spike is initiated only when the current magnitude is more than some threshold value known as *rheobase current*. The time courses of m, h, n are shown in part (b). The sodium current is inward and depolarizes the membrane whereas the potassium current is outward and causes hyperpolarization. It has been observed that the response of n is similar to that of the membrane potential. The value of m jumps to its maximum when this potential crosses a threshold value. Incidentally, the value of h is also high at that time instant. This results in high magnitude of sodium current that leads to a high depolarization. Potassium channel is almost in deactivation state and could not hyperpolarizes the membrane. Therefore a spike is initiated. The rise in membrane potential brings h to a lower value and n to a higher value as seen from the time course of the gating

variables. The membrane potential hyperpolarizes owing to high outward potassium and low inward sodium current. The HH equations model both subthreshold and suprathreshold regime of neuron. This model shows the behavior of Type-II neuron as the firing rate is very high and spike latency is very low [5].

2.2.4 Morris-Lecar Model

FitzHugh and Nagumo *et. al.* reduced the order of HH model and proposed a two dimensional model [12],[27] to make it computationally efficient. Although this model is studied for understanding the dynamics of membrane by several researchers, it has been argued that this model does not represent any practical neuronal membrane. In 1981, Morris and Lecar suggested a two dimensional simplified model that describes the characteristics of barnacle muscle fiber [25]. This model incorporates two ionic currents, one outward going non-inactivating potassium current and the other inward going non-inactivating calcium current. Because calcium current responds much faster than potassium current, it is assumed that calcium current is always in equilibrium for the time scales considered. So, the dynamics of calcium currents can be ignored and the model is reduced to two dimensions. Following equations describe Morris-Lecar model:

$$\begin{aligned} C\frac{dV_m(t)}{dt} &= -\overline{G}_{Ca} m_\infty(V_m)\,(V_m(t) - E_{Ca}) - \overline{G}_K w(t)\,(V_m(t) - E_K) - \\ &\quad G_m\,(V_m(t) - V_{Rest}) + I_{inj}(t) \end{aligned} \tag{2.8}$$

$$\frac{dw(t)}{dt} = \frac{w_\infty(V_m) - w(t)}{\tau_w(V_m)}$$

where $w(t)$ is the recovery variable for potassium channel. The potassium activation variable follows the standard first order equation with steady-state activation

$$w_\infty(V_m) = 0.5\left(1 + \tanh\frac{V_m + 1}{30}\right)$$

The time constant is

$$\tau_w(V_m) = \frac{5}{\cosh(V_m/60)}$$

It is assumed that the calcium current is always at equilibrium, with its activation curve given by

$$m_\infty(V_m) = 0.5\left(1 + \tanh\frac{V_m + 1}{15}\right)$$

There are many variants of the ML model [22]. However, the widely used one considers the following parameter set [35]: $\overline{G}_{Ca} = 1.1, \overline{G}_K = 2.0, G_m = 0.5, E_{Ca} = 100, E_K = -70$, and $V_{rest} = -50$ (all conductances are in mS/cm^2 and potentials in mV). The

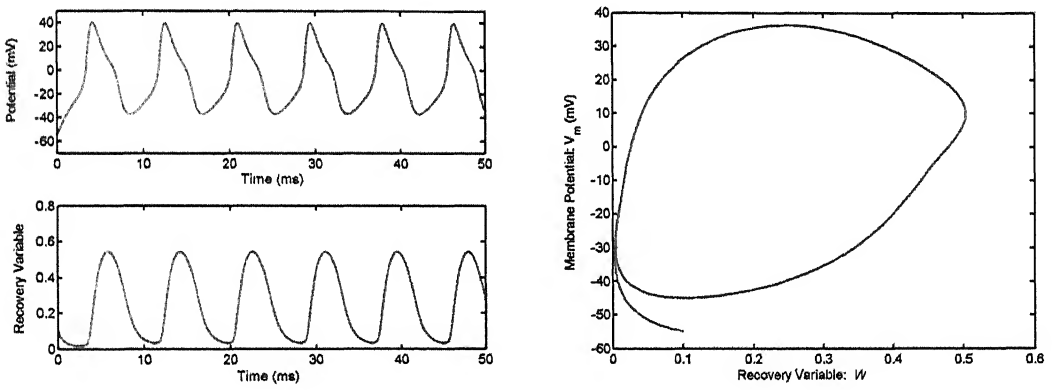

(a) Time course of variables (b) Phase portrait

Figure 2.6: Response of Morris-Lecar model: Case 1

response of the ML model is shown in Figure 2.6. Upper subplot of part (a) shows the firing characteristics. The shape of spike is very sluggish and interspike interval is high. This dynamics represents the properties of Type-I neuron. Lower subplot shows the time course of recovery variable $w(t)$. A phase portrait between the membrane potential $V_m(t)$ and recovery variable $w(t)$ is plotted in part (b). The phase portrait

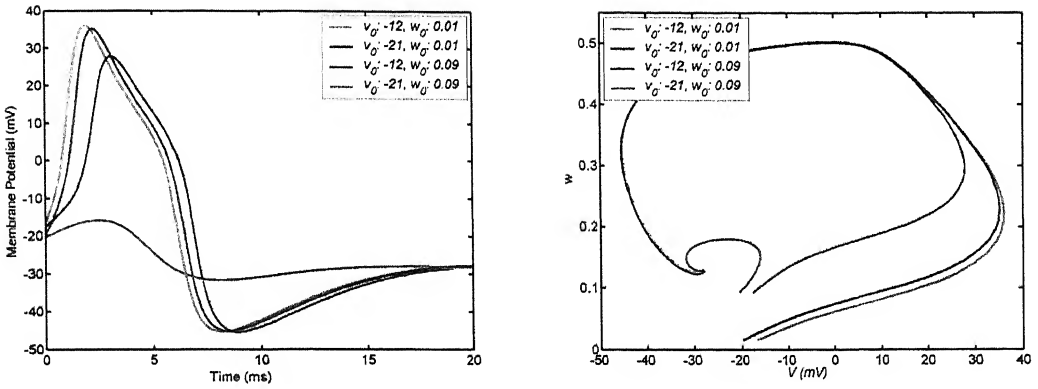

(a) Membrane potential (b) Phase portrait

Figure 2.7: Response of Morris-Lecar model: Case 2

shows a limit cycle. To find out the effect of initial conditions on the ML neuron model, the analysis has een carried out for different initial conditions. The result is shown in Figure 2.7. As depicted from the Part(a) of the figure, there is a fail in generation of action potential (represented by the green line) at some initial condition ($V_m^0 = -21,\ w^0 = 0.09$). Also, the parameter set allows only a single spike irrespective of initial conditions instead of repetitive spiking. The locus of the phase portrait is not a closed one unlike in the case of first parameter set.

2.3 Synapse Modeling

2.3.1 The Synapse

The gap junction between the axon of one neuron and the dendrites of the next neuron is termed as synapse. The synapse allows the transmission of impulse from a neuron to the other. The synapse lies between two terminals called as presynaptic and postsynaptic

terminals. The axon ends at the presynaptic terminal and the dendrites begin from postsynaptic terminal. Synapse is classified as

- Chemical Synapse
- Electrical Synapse

The space between the presynaptic and postsynaptic terminals of the chemical synapse is called the *Synaptic Cleft*. A number of synaptic vesicles exist in the presynaptic terminal. These are spherical membrane bound organelles. Each of the synaptic vesicles contain one or more neurotransmitters. Neurotransmitters are secreted as a form of chemical signals from the presynaptic end. Neurotransmitters work as messengers that convey information from one neuron to the other. The neurotransmitters are classified into two categories – small molecule neurotransmitters and neuropeptides. Small molecule neurotransmitters mediate rapid synaptic actions and neuropeptides tend to modulate slower, ongoing synaptic functions [46].

Even though the chemical synapses outnumber its electrical counterpart, the electrical synapses are found in all nervous systems including human brain [31]. In case of electrical synapse, the membranes of the two communicating neurons come extremely close at the synapse and are actually linked together by an intercellular specialization called a gap junction. Gap junctions contain precisely aligned, paired channels in the membrane of the presynaptic and postsynaptic neurons so that each channel pair forms a pore. A variety of substances diffuse between the cytoplasm of the presynaptic and postsynaptic neurons. Electrical synapses thus work by allowing ionic current to flow passively through the gap junction pores from one neuron to another. The usual source of this current is the potential difference generated locally by the action potential.

2.3.2 Dynamics of Synapse

Synapse transmits the information through synaptic current. The value of current depends on the synaptic conductance $g_{syn}(t)$, synaptic potential E_{syn} and the action

potential $V_m(t)$ arrives at presynaptic terminal. Synaptic current is governed by Equation 2.9

$$I_{syn}(t) = g_{syn}(t)\,(V_m(t) - E_{syn}) \tag{2.9}$$

The presynaptic potential is considered to follow the HH response as shown in Figure 2.5. Chemical synapses are classified as *NMDA Synapse* and *Non-NMDA Synapse* [22]. *NMDA* is the abbreviated form of *N-methyle-O-aspartic acid.* The synaptic conductance for the NMDA synapse is modeled using the Equation 2.10

$$g_{syn}(t) = const \cdot t\; e^{-t/t_{peak}} \tag{2.10}$$

t_{peak} is the time at which the synaptic conductance $g_{syn}(t)$ reaches its maximum value g_{peak}. The value of the constant is $\frac{g_{peak}\; e}{t_{peak}}$. For the values $t_{peak} = 0.5\ ms$ and $g_{peak} = 1\ nS$, the variation in synaptic conductance and synaptic current is plotted in Figure 2.8

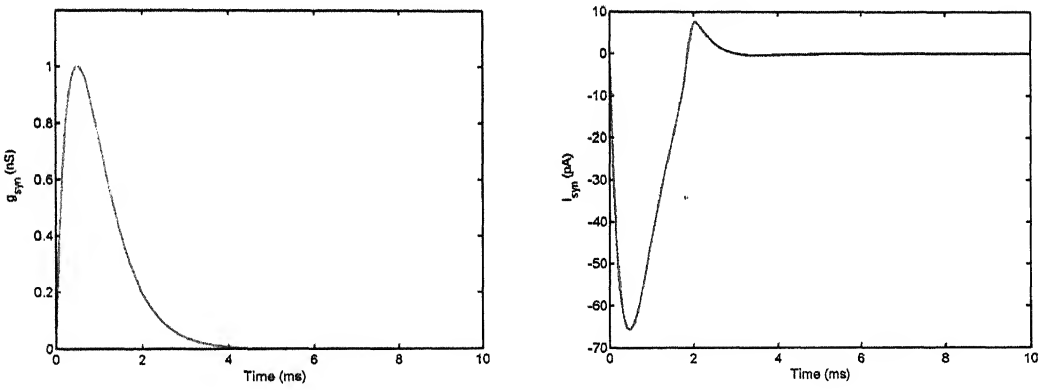

(a) Synaptic conductance (b) Synaptic current

Figure 2.8: Characteristics of NMDA synapse

Major part of the synaptic current lies in the fourth quadrant. Hence, this synaptic current inhibits the next neuron. The value of synaptic conductance rises very fast.

The fall of conductance value is more flat when compared to the rising time. Synaptic current acts like a transient as it falls to zero within a very short period.

The *Non-NMDA* synapse transmits the signal with the help of Mg^{2+} ion. Synaptic conductance is given by,

$$g_{syn}(t) = g_n \frac{e^{-t/\tau_1} - e^{-t/\tau_2}}{1 + \sigma\ [Mg^{2+}]\, e^{-\gamma V_m(t)}} \tag{2.11}$$

The value of g_n varies from 0.2 nS to 0.4 nS at 35^o celsius. Physiological concentration of Mg^{2+} ion is approximately 1 mM. The values of other parameters are $\tau_1 = 145.5\ ms$, $\tau_2 = 4.1\ ms$, $\sigma = 0.33/mM$ and $\gamma = 0.06/mV$. The synaptic current is obtained by directly multiplying the synaptic conductance to the membrane potential as $E_{syn} \approx 0$ [22]. The time course for synaptic conductance and current are shown in Figure 2.9

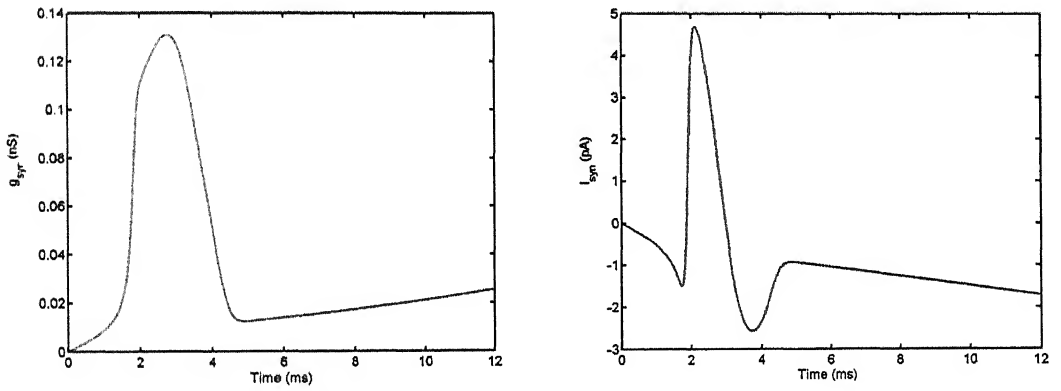

(a) Synaptic conductance (b) Synaptic current

Figure 2.9: Characteristics of Non-NMDA synapse

The Non-NMDA synaptic conductance is a function of action potential. It has a shape similar to a bell-shaped function. The current initially is inhibitory, then an excitatory pulse is generated, and finally it again goes to inhibitory state. However,

this current acts as an excitatory current as the generated pulse is excitatory. The Figure 2.10 shows a current voltage relationship for Non-NMDA synapse. As the spike

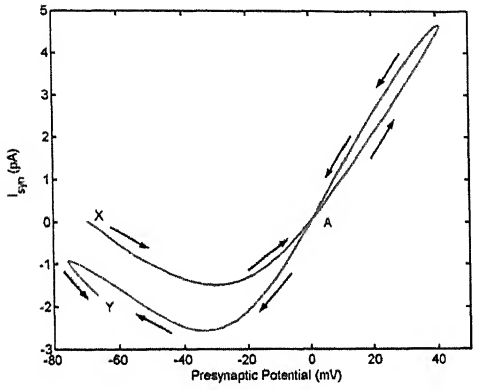

Figure 2.10: Current-voltage relationship for Non-NMDA synapse

falls to the resting potential after it fires as shown in Figure 2.5, the current-voltage relationship shows two values of current for a particular membrane potential. The contour of the curve starts from point X, follows the path shown by arrows and ends at point Y. It intersects itself at Point A. Hence, the value of synaptic conductance is same for both rising and falling edge of spike at this membrane potential. At all other cases, the synaptic conductance does not take the same value for rising and falling edge for any potential value.

2.4 Coupling in Neural Systems

Determining the dynamical behavior of an ensemble of coupled neurons is an important problem in computational neuroscience. From the very beginning of the research in the field of computational neuroscience, people deal with single neuron and its behavior. Present trends of research include investigation of the behavior of neurons considered

in a network and their way to fire synchronously. It is assumed that the activities in the brain are synchronous and underlying interests for synchronization of nonlinear oscillators in physical and biological systems range from novel communication strategies to understand how large and small neural assemblies efficiently and sensitively achieve desired functional goal [30]. The coupling can be linear or nonlinear. The linearity of coupling on a neuron depends on the coupling current introduced by the other neurons coupled to it. Coupling can also be classified as strong and weak based on its strength. The impact of linear coupling on the neuronal behavior will be analyzed in the following sections.

2.4.1 Linear Coupling

The simplest coupling phenomenon is the linear coupling between two neurons. If *Neuron A* and *Neuron B* are coupled with each other, then a current will induced from *Neuron A* to *Neuron B* and vice versa. In case of linear coupling, at any time instant, this current depends directly on the difference between the potentials of the two neurons and the coupling conductance. The coupling conductance determines the strength of the coupling strength. In synaptically coupled neurons, the dynamics of one neuron affects the other only when the potential of that neuron crosses a threshold limit. Morris-Lecar model has been used to find out the coupling effect between neurons. The dynamics of the i^{th} neuron in case of n mutually coupled neurons can be given by Equation 2.12

$$C^i \frac{dV_m^i(t)}{dt} = -\overline{G}_{Ca}^i m_\infty^i(V_m^i)\left(V_m^i(t) - E_{Ca}^i\right) - \overline{G}_K^i w^i(t)\left(V_m^i(t) - E_K^i\right) - C_m^i\left(V_m^i(t) - E_m^i\right) + \sum_{j=1,\ j\neq i}^{n} g_c^{ij}\left(V_m^j(t) - V_m^i(t)\right) H\left(V_m^j(t) - V_{Th}\right) + I_{inj}^i(t) \quad (2.12)$$

$$\frac{dw^i(t)}{dt} = \frac{w_\infty^i(V_m^i) - w^i(V_m^i)}{\tau_w^i(V_m^i)}$$

The *Heaviside Function*, $H\left(V_m^j(t) - V_{Th}\right)$ is used to implement the threshold condition. The activation curve for the calcium and potassium conductance and the time constant used in Equation 2.12 are given by Equation 2.13.

$$\begin{aligned} m_\infty^i &= 0.5\left(1 + \tanh\frac{V_m^i + 1}{15}\right) \\ w_\infty^i &= 0.5\left(1 + \tanh\frac{V_m^i - 10}{14.5}\right) \\ \tau_w^i &= \frac{3}{\cosh\frac{V_m^i - 10}{29}} \end{aligned} \tag{2.13}$$

Table 2.1: Parameter sets for the neurons

Neuron	$\overline{G}_{Ca}$	$\overline{G}_K$	G_M	E_{Ca}	E_K	E_M
Neuron A	1.2	2.0	0.5	120	-84	-60
Neuron B	0.8	2.3	0.6	115	-77	-65
Neuron C	1.0	2.1	0.4	118	-62	-80

It has been assumed that each of the coupled neuron follows Morris-Lecar model as seen from Equations 2.12 and 2.13. This dynamics is found to occur in specific part of brain mostly in the purkinje cell of cortical neuron. However, the parameter values for each neurons are kept different. Owing to nonidentical parameter values, each neuron poses different characteristics such as different firing frequency, rheobase current, and different refractory period. The differences in parameter values occurs due to different ion concentrations even if the neurons are closely located. For the present chapter, the dynamics of three neurons denoted by *Neuron A*, *Neuron B* and *Neuron C* has been considered. The parameter values for the neurons are shown in Table 2.1. The membrane capacitance is assumed to be 1 $\mu F/cm^2$ for all the three neurons. Therefore, the capacitance C is ommited from the equations considered now onwards.

2.4.2 Dynamical Analysis

In order to carry out the dynamical analysis, the equilibrium points are calculated for different stimulus magnitudes. It has been done by forcing the time derivatives of the state variables to zero. By setting $\dot{w^i} = 0$, the value of recovery variable at equilibrium point is obtained as

$$w^{i^*} = w^i_\infty = 0.5\left(1 + \tanh\frac{V^i_m - 10}{14.5}\right)$$

The other condition for the equilibrium is $\dot{V^i_m} = 0$. After substituting the value of w^{i*} in this condition, Equation 2.14 is obtained which when solved gives the value of membrane potential at equilibrium point.

$$-0.5\,\overline{G}^{\,i}_{Ca}\left(1 + \tanh\frac{V^{i^*}_m + 1}{15}\right)\left(V^{i^*}_m - E^i_{Ca}\right) - 0.5\overline{G}^{\,i}_K\left(1 + \tanh\frac{V^{i^*}_m - 10}{14.5}\right)$$
$$\left(V^{i^*}_m - E^i_K\right) - G^{\,i}_m\left(V^{i^*}_m - E^i_m\right) + \sum_{j=1,\ j\neq i}^{n} g^{ij}_c\left(V^{j^*}_m - V^{i^*}_m\right) + I^i_{inj} = 0 \quad (2.14)$$

Equation 2.14 can not be solved explicitly for $V^{i^*}_m$. A numerical approach has been taken to find out the values of $V^{i^*}_m$ for different values of I^i_{inj}. Once the locus of the equilibrium point with respect to current is obtained, the eigenvalues can be calculated to check the stability of the system. Eigenvalues are the roots of characteristic equation

$$det\,|J - \lambda\ I| = 0$$

where J is the *Jacobian Matrix*. Therefore, it is necessary to find out the *Jacobian* to evaluate the eigenvalues. The coupled ML system has the form:

$$\frac{dV^i_m}{dt} = f^i(V^i_m, V^j_m, w^i, w^j)$$

$$\frac{dw^i}{dt} = g^i(V^i_m, V^j_m, w^i, w^j)$$

The *Jacobian* is formed with the values of the derivatives of f^i and g^i with respect to its state variables calculated at its equilibrium point. Therefore, the *Jacobian* is given by,

$$J = \begin{bmatrix} \frac{\partial f^1}{\partial V_m^1} & \frac{\partial f^1}{\partial V_m^2} & \frac{\partial f^1}{\partial V_m^3} & \cdots & \frac{\partial f^1}{\partial w^1} & \frac{\partial f^1}{\partial w^2} & \frac{\partial f^1}{\partial w^3} & \cdots \\ \frac{\partial f^2}{\partial V_m^1} & \frac{\partial f^2}{\partial V_m^2} & \frac{\partial f^2}{\partial V_m^3} & \cdots & \frac{\partial f^2}{\partial w^1} & \frac{\partial f^2}{\partial w^2} & \frac{\partial f^2}{\partial w^3} & \cdots \\ \cdots & \cdots & \cdots & \cdots & \cdots & \cdots & \cdots & \cdots \\ \frac{\partial g^1}{\partial V_m^1} & \frac{\partial g^1}{\partial V_m^2} & \frac{\partial g^1}{\partial V_m^3} & \cdots & \frac{\partial g^1}{\partial w^1} & \frac{\partial g^1}{\partial w^2} & \frac{\partial g^1}{\partial w^3} & \cdots \\ \frac{\partial g^2}{\partial V_m^1} & \frac{\partial g^2}{\partial V_m^2} & \frac{\partial g^2}{\partial V_m^3} & \cdots & \frac{\partial g^2}{\partial w^1} & \frac{\partial g^2}{\partial w^2} & \frac{\partial g^2}{\partial w^3} & \cdots \\ \cdots & \cdots & \cdots & \cdots & \cdots & \cdots & \cdots & \cdots \end{bmatrix}$$

This yields eight types of terms: $\frac{\partial f^i}{\partial V_m^i}$, $\frac{\partial f^i}{\partial V_m^j}$, $\frac{\partial f^i}{\partial w^i}$, $\frac{\partial f^i}{\partial w^j}$, $\frac{\partial g^i}{\partial V_m^i}$, $\frac{\partial g^i}{\partial V_m^j}$, $\frac{\partial g^i}{\partial w^i}$, and $\frac{\partial g^i}{\partial w^j}$. These are given by Equations 2.15 – 2.22.

$$\frac{\partial f^i}{\partial V_m^i} = -0.5\,\overline{G}_{Ca}^i \left(1 + \tanh\frac{V_m^i + 1}{15}\right) - 0.033\,\overline{G}_{Ca}^i \left(1 + \left(\tanh\left(\frac{V_m^i + 1}{15}\right)\right)^2\right) \left(V_m^i - E_{Ca}^i\right) - \overline{G}_K^i\, w^i - G_m^i - \sum_{j=1,\ j\neq i}^{n} g_c^{ij}\, H\left(V_m^j - V_{Th}\right) \quad (2.15)$$

$$\frac{\partial f^i}{\partial V_m^j} = g_c^{ij}\, H\left(V_m^j - V_{Th}\right) \quad (2.16)$$

$$\frac{\partial f^i}{\partial w^i} = -\overline{G}_K^i \left(V_m^i - E_K^i\right) \quad (2.17)$$

$$\frac{\partial f^i}{\partial w^j} = 0 \quad (2.18)$$

$$\frac{\partial g^i}{\partial V_m^i} = 0.012\,\sinh\left(\frac{V_m^i - 10}{29}\right)\left(0.5\,\left(1 + \tanh\frac{V_m^i - 10}{14.5}\right) - w^i\right) + 0.012\,\cosh\left(\frac{V_m^i - 10}{29}\right)\left(1 + \left(\tanh\left(\frac{V_m^i - 10}{14.5}\right)\right)^2\right) \quad (2.19)$$

$$\frac{\partial g^i}{\partial V_m^j} = 0 \tag{2.20}$$

$$\frac{\partial g^i}{\partial w^i} = -0.33 \cosh\left(\frac{V_m^i - 10}{29}\right) \tag{2.21}$$

$$\frac{\partial g^i}{\partial w^j} = 0 \tag{2.22}$$

The *Jacobian* is formed by evaluating Equations 2.15 - 2.22 at the equilibrium points $\left(V_m^{i^*},\ w^{i^*}\right)$. Eigenvalues from *Jacobian* matrix are calculated in order to determine the specific type of bifurcations in system.

2.4.3 Two Neuron Coupling

Consider the coupling between *Neuron A* and *Neuron B* . The independent response of the two neurons are drawn in Figure 2.11 when they are subjected under a stimulus of 20 nA and 35 nA respectively.

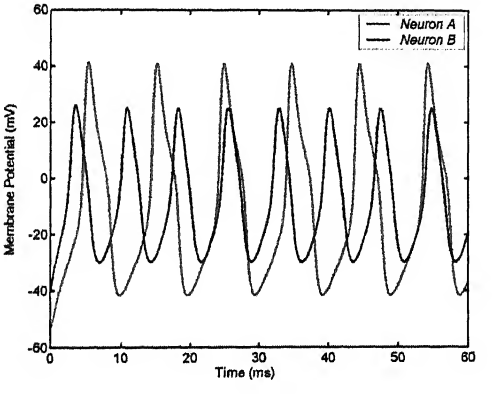

Figure 2.11: Time course of *Neuron A* and *Neuron B* (no coupling)

The red line shows the time course of *Neuron A* and the blue line represents the same of *Neuron B*. It is observed here that the interspike interval of *Neuron A* is much

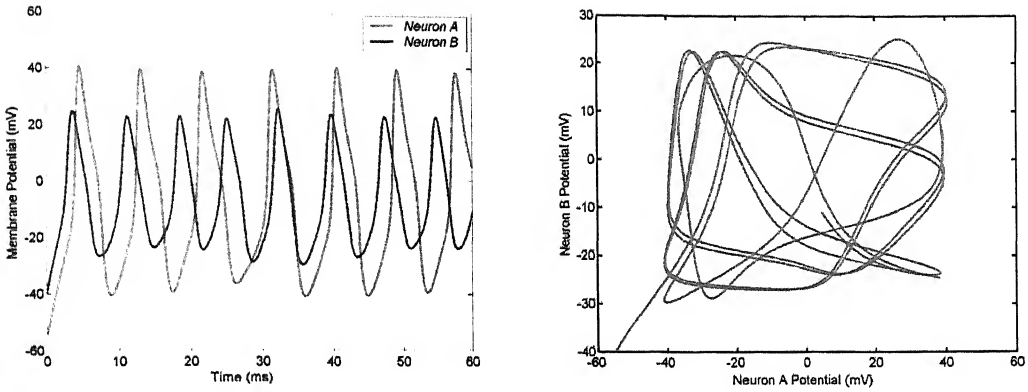

(a) Time course of membrane potentials (b) Phase portrait

Figure 2.12: Response of weakly coupled neurons

larger when compared with that of *Neuron B*. The response for the coupled model with coupling conductance $g_c^{12} = g_c^{21} = 0.1\ mS/cm^2$ is plotted in Figure 2.12. It is found that *Neuron A* and *Neuron B* try to synchronize with each other as the difference in their firing frequencies reduces to 29.73 Hz from 33.96 Hz. The phase portrait between the membrane potential of each neuron is plotted in Part (b). To achieve synchronization, the firing frequency of the two neurons should be same and therefore the phase portrait between the membrane potentials must yield a straight line. An increase in coupling strength may drive the neurons into synchronism. The behavior of the neurons are studied for $g_c^{12} = g_c^{21} = 0.8\ mS/cm^2$ and the results are shown in Figure 2.13. It is evident that the strongly coupled neurons are almost in synchronism. The two neurons fire together with a frequency of $121.5Hz$.

The variation in the behavior of the neurons has been observed by plotting bifurcation diagram at different injected current. Two cases are considered, one with $g_c^{12} = 0.1\ mS/\mu m^2$ for weak coupling and the other with $g_c^{12} = 0.8\ mS/\mu m^2$ for strong coupling. The stimulus magnitudes are assumed to be identical for both the neurons,

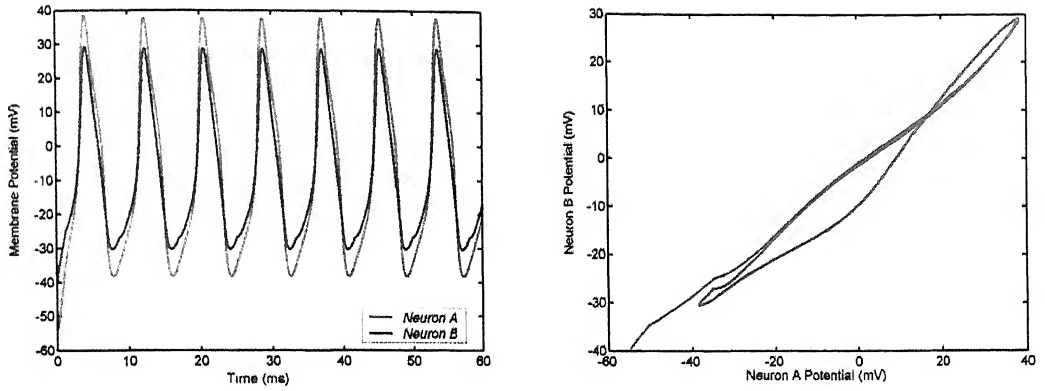

(a) Time course of membrane potentials (b) Phase portrait

Figure 2.13: Response of strongly coupled neurons

i.e. $I_1^{inj} = I_2^{inj} = I$. The system has four system states and the state vector is given by,

$$X = \left[V_m^1 \; V_m^2 \; w^1 \; w^2\right]^T$$

Owing to its four dimensionality, it has four eigenvalues for each equilibrium point. The equilibrium point shifts as the magnitude of stimulus is varied. This results in a change of the eigenvalues with respect to stimulus which helps to describe the system dynamics at the equilibrium point. Part(a) of Figure 2.14 plots the locus of eigen values with respect to stimulus. Two (λ_1, λ_2) of the four eigenvalues are pure real and the other two (λ_3, λ_4) are complex conjugates. The magnitude of real part of λ_1, and λ_2 crosses the zero value for $I = 12.95$. The other two eigenvalues remain positive. This condition shows the existence of *Hopf Bifurcation*. The equilibrium points and eigenvalues for the corresponding stimulus are given in Table 2.2

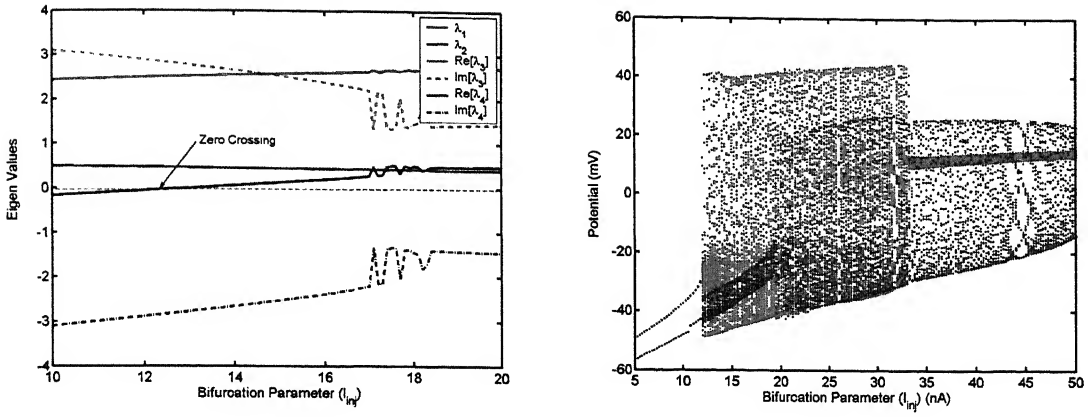

(a) Locus of eigenvalues (b) Bifurcation diagram

Figure 2.14: Bifurcation analysis for two weakly coupled neurons

Table 2.2: Values for weakly coupled neurons

State	Equilibrium Point	Eigen Value
V_m^1	7.74	2.52
V_m^2	34.46	0.46
w^1	0.43	0 + j 2.78
w^2	0.97	0 - j 2.78

The *Jacobian* at equilibrium point for the stimulus at bifurcation point is

$$J_{g_c^{12}:0.1} = \begin{bmatrix} 3.31 & 0.1 & -183.48 & 0 \\ 0.1 & 0.46 & 0 & -256.37 \\ 0.01 & 0 & -0.33 & 0 \\ 0 & 0.03 & 0 & -0.46 \end{bmatrix}$$

The bifurcation diagram portraits the change in system state when the bifurcation parameter is varied. The height at any particular point shows the change in magnitude between two time instants at that value of bifurcation parameter. Therefore, the system behavior changes with the sudden increase of height from a very low value. In the Part(b) of Figure 2.14, red dots show the bifurcation of *Neuron A* and the same for the *Neuron B* is shown by blue dots. There is a behavioral change, i.e. transition from stable to oscillatory mode at $I = 12.95\ nA$. The result is a *Hopf Bifurcation.* However, the response of the *Neuron B* is not identical with that of *Neuron A* due to the weak coupling of neurons. Bifurcation Analysis is carried out for strongly coupled neurons

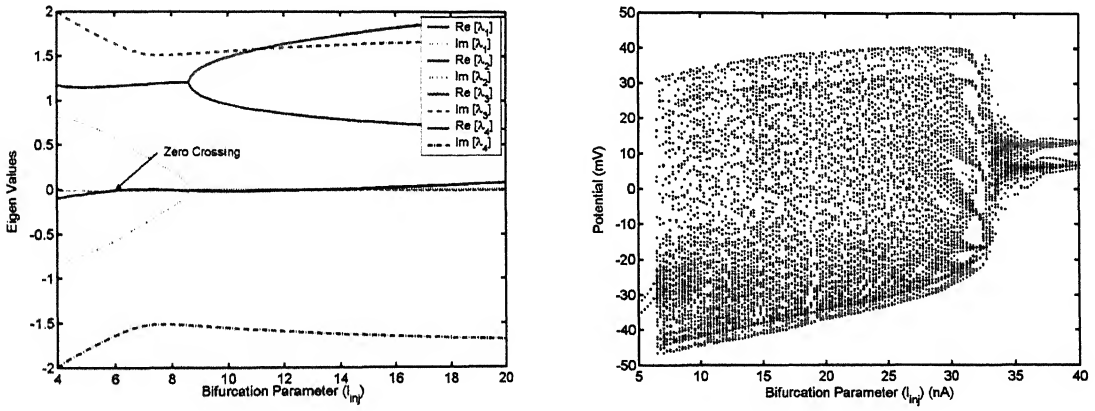

(a) Locus of eigenvalues (b) Bifurcation diagram

Figure 2.15: Bifurcation analysis for two strongly coupled neurons

and the response is shown in Figure 2.15. The real parts of a complex conjugate eigenvalues cross the zero value for $I = 6.31\ nA$. Hence, the *Hopf Bifurcation* occurs at this value of current. The system moves from the stable state to oscillatory state. This is also evident from the bifurcation diagram. The red and blue dots show the responses for *Neuron A* and *Neuron B* respectively. The distribution of red and blue dots are equally dense as the system is synchronized because of strong coupling between them. Table 2.3 shows the eigenvalues and the equilibrium points. The *Jacobian* for $I = 6.31\ nA$ is computed as

$$J_{g_c^{1,2}:0.9} = \begin{bmatrix} 2.35 & 0.8 & -175.25 & 0 \\ 0.8 & 0.65 & 0 & -208.39 \\ 0.01 & 0 & -0.34 & 0 \\ 0 & 0.01 & 0 & -0.34 \end{bmatrix}$$

Table 2.3: Values for strongly coupled neurons

State	Equilibrium Point	Eigen Value
V_m^1	3.63	1.17 + j 0.52
V_m^2	13.6	1.17 - j 0.52
w^1	0.29	0 + j 1.59
w^2	0.62	0 - j 1.59

2.4.4 Three Neuron Coupling

In this section, the coupling behaviors of three neurons, *Neuron A, Neuron B* and *Neuron C* are analyzed in order to find out the effect of increased population on coupling. Stimulus applied to *Neuron A* and *Neuron B* are identical to earlier two neuron coupling model, *i.e.* 20 nA and 35 nA respectively. *Neuron C* is subjected under a current

of magnitude 10 nA. The parameters of *Neuron C* are chosen in a way such that it remains in the subthreshold regime for lower stimulus magnitude. The idea behind this is to find out the effect of coupling on neurons that do not fire under normal conditions. The independent uncoupled response of the three neurons are shown in Figure 2.16. As mentioned before, the *Neuron C* could not cross the threshold and hence no spike is initiated in it (black line).

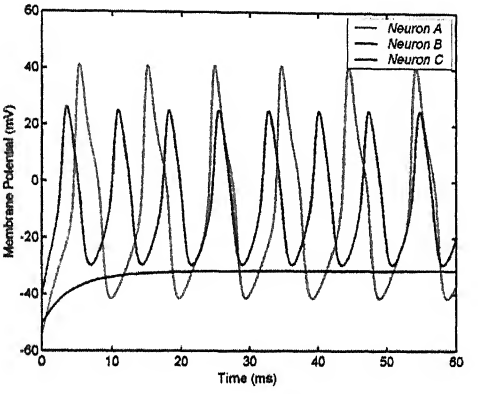

Figure 2.16: Time course of *Neuron A, Neuron B* and *Neuron C* (no coupling)

If the neurons are coupled together with a very low coupling conductance $g_c^{ij} = 0.1\ mS/cm^2$, the third neuron crosses the subthreshold regime and starts firing. However, the whole system is highly unsynchronised as depicted from the randomness of the phase portrait shown in Figure 2.17. Time courses of the neurons also show different firing frequencies. The *Neuron B* has highest firing rate followed by *Neuron A*. Although *Neuron C* exhibits firing, it has the lowest firing frequency. Therefore, the *Neuron C* needs more coupling current to fire synchronously with the other two.

The coupling conductance for the three weakly coupled neuron model has the same magnitude of that of two weakly coupled model. The phase portrait between *Neuron A* and *Neuron B* is less random in the present condition when compared with the two

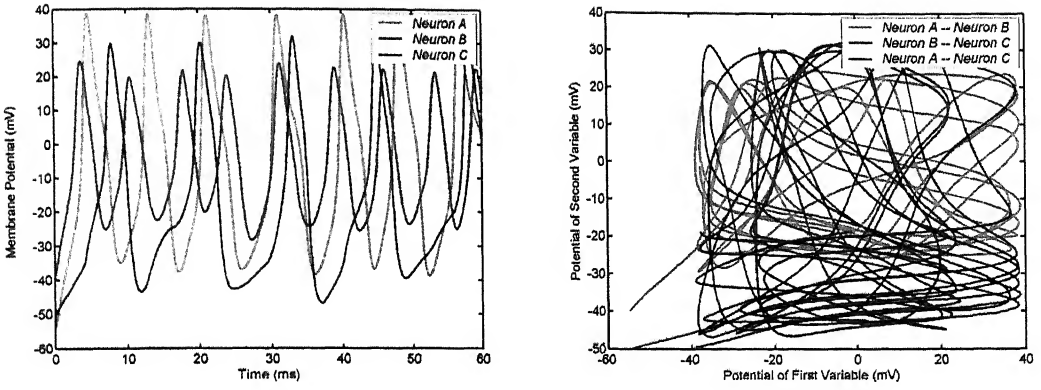

(a) Time course of membrane potentials (b) Phase portrait

Figure 2.17: Response of three weakly coupled neurons

neuron model. Similarly the firing frequency difference between *Neuron B* and *Neuron A* is slightly less (lesser by 1.57 Hz from two neuron case) in three neuron model. It can be concluded that the introduction of third neuron affects, though not in great extent, the synchronization between other two neurons.

The next objective is to find out whether a higher coupling strength brings *Neuron C* into synchronism like the earlier two neuron coupling model. The coupling conductance has been increased to 0.8 mS/cm^2. The neurons are now synchronized with each other. All the three neurons fire with a frequency of $109.82Hz$. The phase portrait between two neurons considered at a time is almost linear. Therefore the coupling also synchronizes the neurons that are uncapable to cross the subthreshold regime. The response is shown in Figure 2.18.

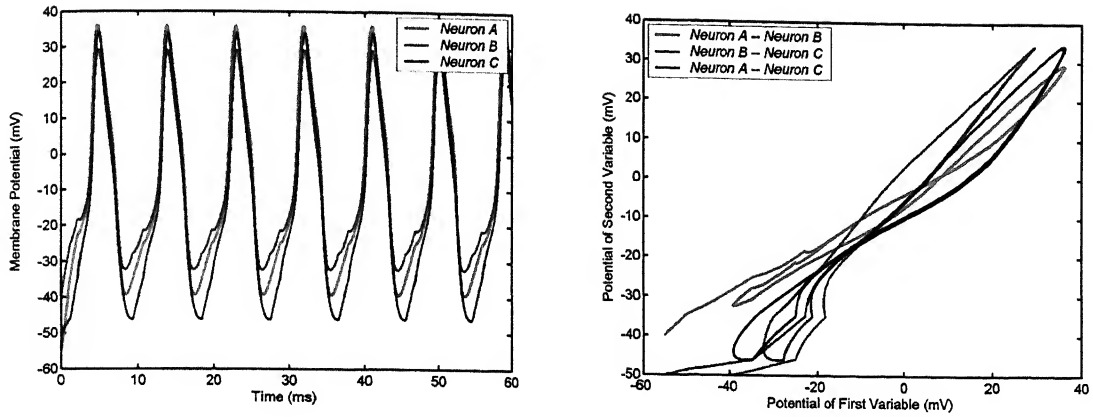

(a) Time course of membrane potentials (b) Phase portrait

Figure 2.18: Response of three strongly coupled neurons

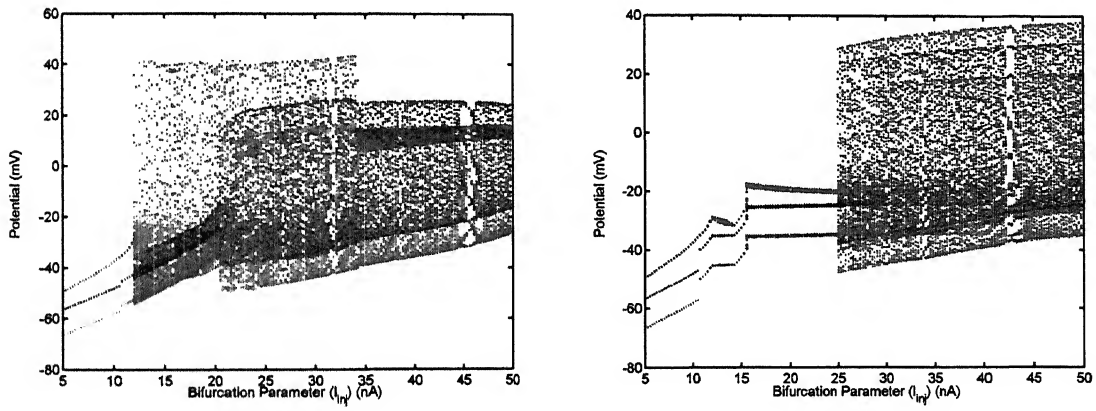

(a) Weak Coupling (b) Strong Coupling

Like the two coupled neuron model, a bifurcation analysis is carried out for the present model. The stimulus has been considered as the bifurcation parameter. It is varied in steps to find out the changes in the behavior of the systems. A bifurcation diagram is drawn in Figure 2.19 with respect to stimulus magnitude. The red, blue and green dots show the membrane potential of *Neuron A*, *Neuron B* and *Neuron C* respectively. The coupled system enters in to oscillatory state from converging state at a current of 11.75 nA for weakly coupled and 24.8 nA for strongly coupled neurons. The diagram shows presence of *Hopf Bifurcation.*

2.5 Summary and Conclusion

In this chapter, the architecture and functions of a neuron and its different parts are described. The neurons are classified based on its topology, functioning and dynamical behavior. Characteristics of a passive membrane is studied. Response of *Type-I* and *Type-II* neuron models are analyzed. The effect of initial condition is studied for *Type-I* neuron model. The Morris-Lecar neuron model shows a *Type-I* behavior whereas the Hodgkin-Huxley neuron model has a *Type-II* characteristics. The neuron models may exhibit a periodic spiking as well as a single spike. For any magnitude of stimulus, the neuron may and may not fire depending upon its initial conditions given by resting potential and the ion conductance at that potential. Synaptic response for both *NMDA* and *Non-NMDA* synapse are observed. For a presynaptic potential that follows HH characteristics, the synaptic current is found to be inhibitory in case of *NMDA* synapse and excitatory in case of *Non-NMDA* synapse. Finally, the behavior when two and three neurons are coupled together has been examined. The magnitude of coupling strength affects the synchronization between the neurons. It is possible that a neuron may fire synchronously with other neurons even if it is uncapable to fire under lower stimulus magnitude. The coupling currents from other neurons help to fulfill the current deficiency required to fire the neuron. A bifurcation analysis has been carried out on

coupled neuron models to find out the effect of stimulus. The coupled neurons enter to oscillatory mode for the equal magnitude of current. However, in case of weakly coupled neurons, there exist a frequency difference between the firing of neurons unlike the strongly coupled neurons. The dynamical analysis show that the excitability of neurons are very much dependent upon the coupling strengths. The magnitude of coupling strength also shifts the bifurcation point. These dependencies have to be taken care while implementing the coupling phenomenon in real systems.

Chapter 3

Signal Propagation in Neuron

The communication occurs in nervous system by the means of electrical signal. A neuron comprises of dendrites, soma and an axon. The dendrites receive electrical signals as a form of current from synapse. These current signals change the potential of dendritic membrane. Now the signals propagates down the dendrites as a form of voltage and summed up at soma. The aggregated potential is transferred to *Axon hillock* though a conductance. The current at *Axon hillock* initiates an *Action Potential* that travels along the axon which again converts into current signal at synapse that excites the dendrites of next neuron. Therefore, studying the phenomenon of signal propagation is very important in order to understand the behavior of nervous system.

3.1 Cable Theory

3.1.1 Cable Equation

The dendrites and axon have a shape similar to a tapered cylinder. They are referred as cable owing to their cylinder-like structure. Since the diameter of this cylinder is very small, there is physically no variation in potential along the cross-section of it. However, the potential gets delayed in both active and passive membrane and decayed

in case of passive membrane as it propagates. The delay depends on its propagation speed. The decay in passive membrane occurs due to the longitudinal resistance of the cable. The passive membrane does not have any ion channels embedded in it that prevents the attenuation. The working of axon and dendrites are explained with the help of cable theory. The cable equation is given by,

$$C\frac{\partial V_m(x,t)}{\partial t} = \frac{1}{2ar_L}\frac{\partial}{\partial x}\left(a^2\frac{\partial V_m(x,t)}{\partial x}\right) - i_m(x,t) + I_{inj}(x,t) \tag{3.1}$$

where r_L is the intracellular resistivity and a is the radius of cable. The membrane current i_m may follow either the Hodgkin-Huxley dynamics or simple passive membrane model depending upon the part of neurons considered. The Equation 3.1 is reduced to Equation 3.2 when the cable has uniform cross-section.

$$C\frac{\partial V_m(x,t)}{\partial t} = \frac{a}{2r_L}\frac{\partial^2 V_m(x,t)}{\partial x^2} - i_m(x,t) + I_{inj}(x,t) \tag{3.2}$$

In case of passive membrane, the membrane current is given by $i_m(x,t) = V_m(x,t)/R_m$, where R_m is membrane resistance. This reduces the cable equation to

$$CR_m\frac{\partial V_m(x,t)}{\partial t} = \frac{aR_m}{2r_L}\frac{\partial^2 V_m(x,t)}{\partial x^2} - V_m(x,t) + I_{inj}(x,t)R_m \tag{3.3}$$

The potential is a function of time and space. The passive membrane does not have any ion pumps embedded in it that prevents the decay in potential. Therefore the passive membrane potential is attenuated both with respect to time and space. This potential has a time constant $\tau = CR_m$ and space constant $\xi = \sqrt{\frac{aR_m}{2r_L}}$. A typical membrane has a time constant $\tau = 1-2\ ms$ [22] and space constant $\xi \approx 1\ mm$ [9]. The signal is offered a resistance when it travels longitudinally. This longitudinal resistance is given by $R_\xi = \frac{R_m}{2\pi a\xi} = \frac{r_L\xi}{\pi a^2}$. The analytical solution for the passive membrane model may be found out for some current waveforms.

The constant current injection of magnitude I_e yields a solution given by,

$$V_m(x) = \frac{I_e R_\xi}{2} e^{-x/\xi}$$

The active membranes like axon that have ion pumps embedded to facilitate the propagation can not be solved analytically as the dynamics of ion channels introduce high nonlinearity in it. Hence a numerical approach (multicompartment model) is used to model axon or dendrites.

3.1.2 Multicompartment Model

This is a numerical method to compute the action potential. Instead of considering the axon or dendrite as a whole, they are split in to many segments. Each segment has a very small length and therefore assumed to be equipotential along its length. In other words, the potential does not change along the length of each compartment considered separately. Two successive compartments are coupled with a conductance and hence the potential differs due to drop in the conductance. The ion pumps modeled by HH equations inject current in order to prevent the decay in action potential so that it can propagates down to the presynaptic terminal. The current equation for the μ^{th} compartment is given by Equation 3.4

$$C\frac{dV_m^\mu(t)}{dt} = -i_m^\mu(t) + g^{\mu,\mu-1}\left(V_m^{\mu-1}(t) - V_m^\mu(t)\right) + g^{\mu,\mu+1}\left(V_m^{\mu+1}(t) - V_m^\mu(t)\right) + I_{inj}^\mu(t) \quad (3.4)$$

The coupling conductance between two successive compartments μ and μ' is

$$g^{\mu,\mu'} = \frac{a^\mu a^{\mu'^2}}{r_L L^\mu \left(L^\mu a^{\mu'^2} + L^{\mu'} a^{\mu^2}\right)}$$

where a^μ is radius and L^μ is the length of the μ^{th} compartment. Owing to very small length of each compartment, the variation in potential across the length of compartment is negligible. Thus the spatial derivative of the potential vanishes from Equation 3.4. The partial differential equation resolves into N coupled nonlinear differential

quations. In order to find out the solution of Equation 3.4, the potential of the $(\mu+1)^{th}$ ompartment at the same time instant must be known. Therefore, an implicit method uch as *Backward Euler* or *Crank Nicholson Method* may be used. The first method s more stable whereas the second is more accurate. The results are shown from the nalysis carried out with *Crank Nicholson Method.* The *Backward Euler* method and *Crank Nicholson* method are described in Appendix-A.

3.2 Dendritic Propagation

The dendrites do not contain any ion pumps. They are modeled using a capacitor n parallel with a resistance. Owing to its passive nature, the signal attenuates as t propagates toward soma. The dendrites are very small in length and larger in ross-sectional area. Hence the attenuation does not result in complete die out of ignal. The potential reached at soma from different dendrite terminals are aggregated ogether that stimulate the *Axon hillock* which in turn initiate the action potential. The dynamics of the dendrite is governed by Equation 3.5

$$C\frac{\partial V_m(x,t)}{\partial t} = \frac{a}{2r_L}\frac{\partial^2 V_m(x,t)}{\partial x^2} - \frac{V_m(x,t) - V_{Rest}}{R_m} + I_{inj}(x,t) \tag{3.5}$$

The break up of dendrites into small compartments results in to the change of he Equation 3.5 to Equation 3.6 for the μ^{th} compartment. The synaptic current is ulsative in nature as observed from Figure 2.8 and 2.9. The response of a dendrite ubjected under a pulse current is shown in Figure 3.1. The major part of the den- rites lies in synaptic area. This helps stimulus not only to be injected at the dendritic erminal, but also to spread along its stem. This in turn reduces the decay of signal. In he simulation, different fractions of stimulus are injected from first to third compart- nent. The potentials show sharp peaks for these compartments as seen from Figure 3.1 nd for the later compartments, the peaks are smoother. If the dendrites would have een stimulated only at the first compartment, the decay results in complete die out

of potential.

$$c\frac{dV_m^\mu(t)}{dt} = g^{\mu,\mu-1}\left(V_m^{\mu-1}(t) - V_m^\mu(t)\right) + g^{\mu,\mu+1}\left(V_m^{\mu+1}(t) - V_m^\mu(t)\right) - \frac{V_m^\mu(t) - V_{Rest}}{R_m} + I_{inj}^\mu(t) \tag{3.6}$$

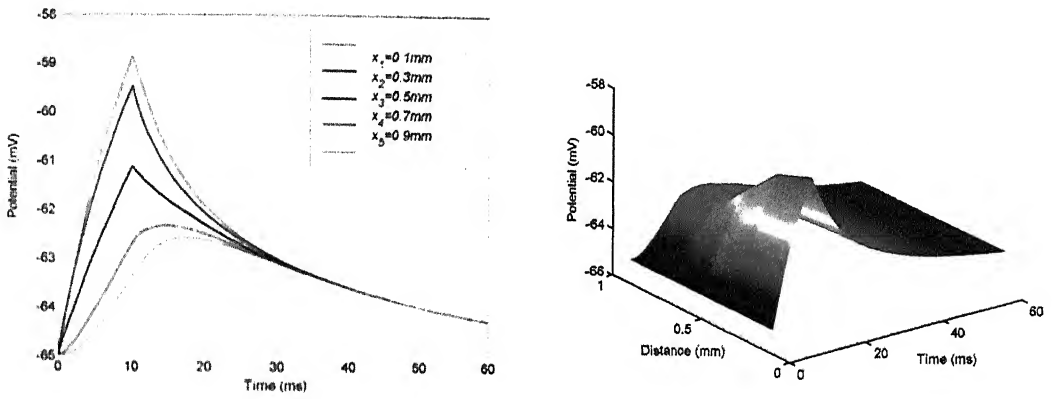

(a) At different locations with respect to time (b) Three dimensional plot

Figure 3.1: Signal propagation in dendrite

3.3 Axonal Propagation

The signal in membrane are of two types – Graded Potential and Action Potential. Graded potentials are short lived depolarizations or hyperpolarizations of an area of membrane. These changes cause local flows of current that decrease with distance. Axon is very long in length and hence the graded signal die out completely if it travels down the axon. To transmit the information from a neuron to other, the *Axon hillock* generates action potential. The generation and transmission of action potential is facilitated by the ion pumps embedded in it.

3.3.1 Propagation of Action Potential

In order to find out the behavior of action potential when it travels down the axon, a multicompartmental analysis is carried out. The axon that has been considered for analysis has a length of 12 cm and a tapering cross-section with the diameter varies from 8 μm near soma to 2 μm at its end. It has been split into 25 compartments. The action potential $V_m^{\mu}(t)$ at μ^{th} compartment follows Equation 3.4. The result is shown in Figure 3.2

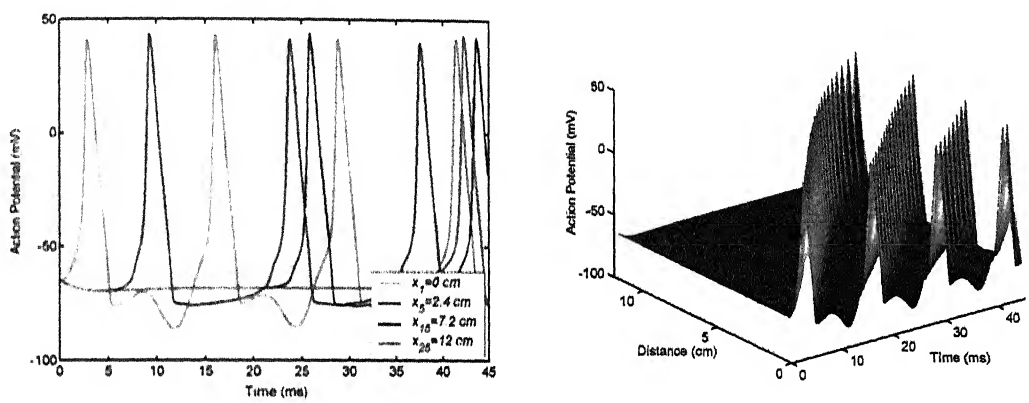

(a) At different locations with respect to time (b) Three dimensional plot

Figure 3.2: Action potential propagation in axon

As observed from the figure, the spikes at the distant locations occur at a later time instant. Thus the action potential is delayed and occur at a later time. The shape and magnitude of the potential is identical except small perturbations like slight increase or decrease in magnitudes, more or less sharpness etc. The uneven ion concentrations in different ion channels are responsible for these perturbations.

3.3.2 Noise in Axon

Under normal conditions, a minimum value of current is required to generate an action potential. For the topology of axon considered, an action potential is fired for $I^0_{inj} = 11\ nA$ and it travels down the axon without being attenuated. If the current injection at *Axon hillock* reduces to $10\ nA$, the action potential fails to generate as shown in Figure 3.3. However, there may still be a chance that the action potential is generated if it suffers by noise. Noise may be a result of either of the two or both reasons mentioned below.

- Uneven opening and closing of gates of ion channels embedded on axon
- Ephaptic Interaction [18] by a nearby axon.

The noise is assumed to follow a *Gaussian* distribution with zero mean and unity variance *i.e.* a white gaussian noise. The stochastic multicompartment model of axon is given by Equation 3.7

$$c\frac{dV^{\mu}_m(t)}{dt} = -i^{\mu}_m(t) + g^{\mu,\mu-1}\left(V^{\mu-1}_m(t) - V^{\mu}_m(t)\right) + g^{\mu,\mu+1}\left(V^{\mu+1}_m(t) - V^{\mu}_m(t)\right) + I^{\mu}_{inj}(t) + \eta^{\mu}(t) \quad (3.7)$$

$$I^{\mu}_{inj}(t) = 0 \quad if\ \mu \neq 1$$

The probability of occurring action potential has been found out for a range of noise intensity with power output varying from 1 dBW to 5 dBW. The results are shown in Table 3.1. The part(b) of the Figure 3.3 shows the generation of action potential at $I = 10\ nA$ with 4 dBW noise power. It is clear from the table that noise does not affect the generation of action potential to a great extent. The 5 dBW white gaussian noise initiates an action potential if the current at axon hillock is just lesser than the threshold current required for generation. However, it fails to do the same if the current drops to 9 nA. Therefore the system is very less prone to noise and the system is robust. There would not be a false firing when the signal is lower than the threshold condition.

Table 3.1: Effect of noise power on generation of action potential

Samples	Noise Power (dBW)	Spike Initiation		%Spiking	
		$I_{inj} = 10\ nA$	$I_{inj} = 9\ nA$	$I_{inj} = 10\ nA$	$I_{inj} = 9\ nA$
50	1	18	0	36	0
	2	15	0	30	0
	3	24	0	48	0
	4	29	4	58	8
	5	39	3	78	6

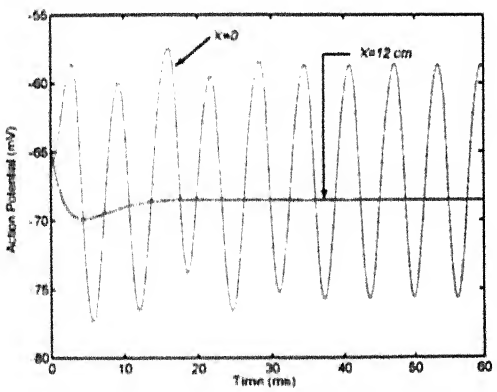

(a) No noise

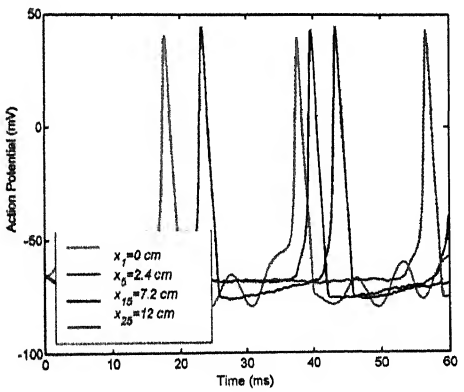

(b) With 4 dBW noise power

Figure 3.3: Action potential at $I = 10\ nA$

3.4 Fourier Analysis

The multicompartment model is very complex. It requires implicit method for analysis and the stability of the solution depends on many factors *viz.* integration time step, number of compartments and type of method. The shape of the action potential does not change with time. The propagation introduces only delay. It has been considered in spiking neuron model that the shape of action potential does not contain any information. The drawbacks of multicompartment model along with this phenomenon is the inspiration of *Fourier Analysis*. The Fourier analysis can be performed only in periodic waveforms. The spike-diffuse-spike model, which is observed numerically in more detailed biophysical models, has periodic traveling wave solutions [8]. The Figure 3.2 also shows the periodic nature of action potential. Therefore the action potential can be modeled using Fourier series. The point neuron HH model has been decomposed into a series combination of sinusoidal terms. These terms are modified with proper transformation in order to achieve the waveform similar to that of an action potential.

3.4.1 Fourier Representation of Hodgkin-Huxley Neuron Model

The dynamics of HH model is governed by Equation 2.7. Simulations have been carried out for different values of injected current ranging from 10 nA to 40 nA. It is found that the frequency of the spiking increases with the increment in the magnitude of the injected current. As the frequency plays an important role in the decomposition of any periodic waveform into Fourier components, an estimation of time period for different current injection is necessary. It has been found that the repetitive spiking occurs at a current value larger than 9 nA. A parabolic curve approximates the interspike interval (ISI) for different current values. The curve suggested here is given by,

$$ISI = (13 - \sqrt{1.32(I_{inj}(t) - 9)}\,)H(I_{inj}(t) - 9) \tag{3.8}$$

Heaviside function is used to take care that the Fourier series method is applied

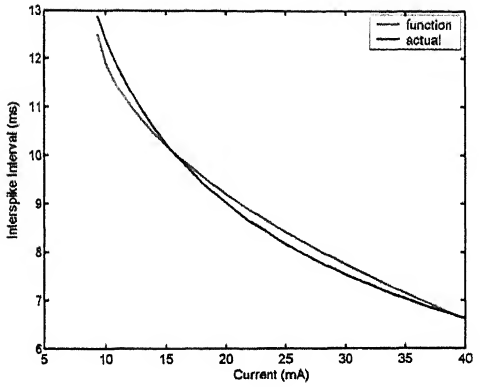

Figure 3.4: Interspike interval as a function of injected current

only in case of repetitive spiking. Figure 3.4 demonstrates that the curve given by Equation 3.8 can be used as an approximator of the time period. The blue line in the figure represents the actual curve of the time period for different current injection in HH model and the trajectory of the parabolic curve (approximated curve) is shown by the red line.

The Fourier series of a function $f(t)$ with time period $2l$ is given by Equation 3.9

$$f(t) = \frac{a_0}{2} + \sum_{k=1}^{\infty} a_k cos\frac{k\pi t}{l} + \sum_{k=1}^{\infty} b_k sin\frac{k\pi t}{l} \tag{3.9}$$

where,

$$\begin{aligned} a_0 &= \frac{1}{l}\int_0^{2l} f(t)dt; \\ a_k &= \frac{1}{l}\int_0^{2l} f(t)cos\frac{k\pi t}{l}dx; \\ b_k &= \frac{1}{l}\int_0^{2l} f(t)sin\frac{k\pi t}{l}dx \end{aligned} \tag{3.10}$$

Equation 3.10 considers the case when the function value is known in the domain 0 to $2l$. The HH equations are coupled differential equations and hence the function $f(t)$ is not known explicitly. However, the value of the membrane potential at different intervals can be obtained by solving the HH model numerically. Hence, to find out

values of a_0, a_k and b_k, the integrals have to be subdivided into many intervals for which the value of membrane potential is known. Each of the integrals can be integrated numerically and added together to get the value of the coefficients. The *Simpson's* 1/3 rule is used for the analysis as it is very simple and also gives fairly good results.

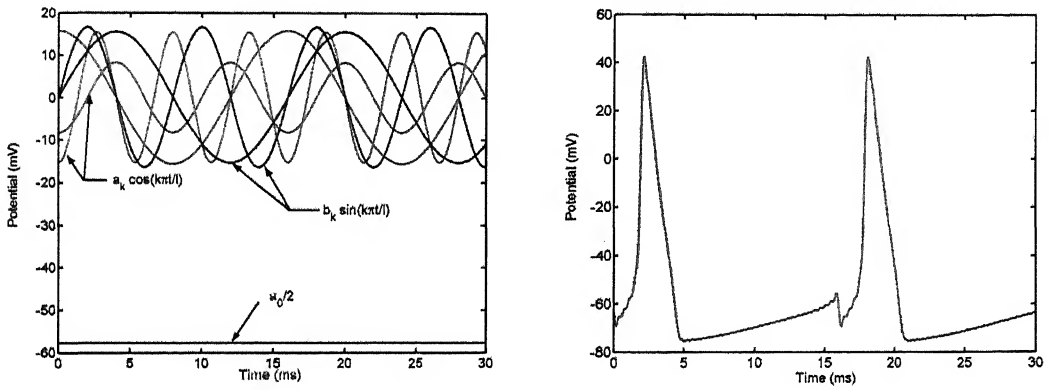

(a) Individual Fourier components (b) After aggregation

Figure 3.5: Membrane potential with Fourier analysis

Figure 3.5 shows the response after the Fourier analysis for a current injection of 10 nA. With the help of numerically calculated Fourier components, the coupled nonlinear differential equations are represented algebraically.

3.4.2 Constructing Action Potential

Equation 3.1 is a partial differential equation in which the dependent variable action potential is a function of both time and space. The equation represents a wave.

A wave that travels at a speed c in the x direction may be represented as

$$V_m(x,t) = V_m(ct - x) \tag{3.11}$$

The Fourier coefficients are obtained for the point neuron model. These coefficients can be used in a tactical way to compose a wave. The proposed model to generate the action potential is given by Equation 3.12

$$V_m(x,t) = \frac{a_0}{2} + \sum_{k=1}^{\infty} a_k cos\left(k\left(ct - x\right)\right) + \sum_{k=1}^{\infty} b_k sin\left(k\left(ct - x\right)\right) \tag{3.12}$$

Equation 3.12 introduces the delay depending upon the speed of the propagation as the action potential moves along the axon. There is no attenuation and change of shape. It is solved numerically to obtain the final response of the propagating signal. The response is shown in Figure 3.6

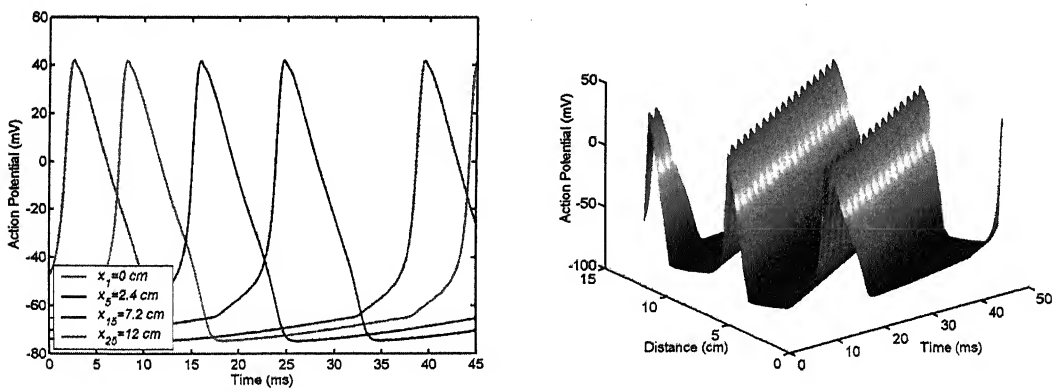

(a) With respect to time at different locations (b) Three dimensional plot

Figure 3.6: Action potential with Fourier analysis

The response is similar to that of multicompartmental model shown in Figure 3.2. However, there are some drawbacks in this Fourier series method. These are –

- The shape of the spike slightly detoriates. It becomes more flat unlike the sharp spike of action potential obtained from the multicompartment model.
- The response shows an existence of spike at axon end before the occurrence of spike near axon hillock. This has to be eliminated in order of proper functioning of the model.

The advantage of this model is that it is very simple and can be used robustly if the initial spike at axon end is suppressed.

3.5 Analysis on Complete Neuron Structure

The researches in Computational Neuroscience are carried out on point neuron model, dendrites, axon and synapse separately. The focus on the complete structure of the neuron has till now got very less significance. The dynamics of complete neuron is very much important for population analysis.

3.5.1 Structure of model

The neuron is considered to have three dendrites – *Dendrite A*, *Dendrite B*, and *Dendrite C*. *Dendrite A* and *Dendrite B* are assumed to receive the signal from *Synapse A* whereas *Dendrite C* receives signal from *Synapse B*. *Synapse A* is a *Non NMDA Synapse* and *Synapse B* is an *NMDA Synapse*. Furthermore, it has also been assumed that the dendrites are closely located and therefore no significant resistance exists between two dendrites. The signals from synapse propagate through dendrites and are summed up at soma. This generates an action potential at *Axon hillock*. The axon is considered to be unbranched.

Two cases have been considered when the axon terminates at synapse. Analysis on the model has been carried out for each part separately. The cases are –

- Termination at *Synapse C* with characteristics similar to that of *Synapse A*.
- Termination at *Synapse D* with characteristics similar to that of *Synapse B*.

3.5.2 Dendrites

The dendrites are modeled as a passive membrane. As discussed earlier, the dendrites take inputs from two synapses. The waveform of synaptic current is shown in Figure 3.7

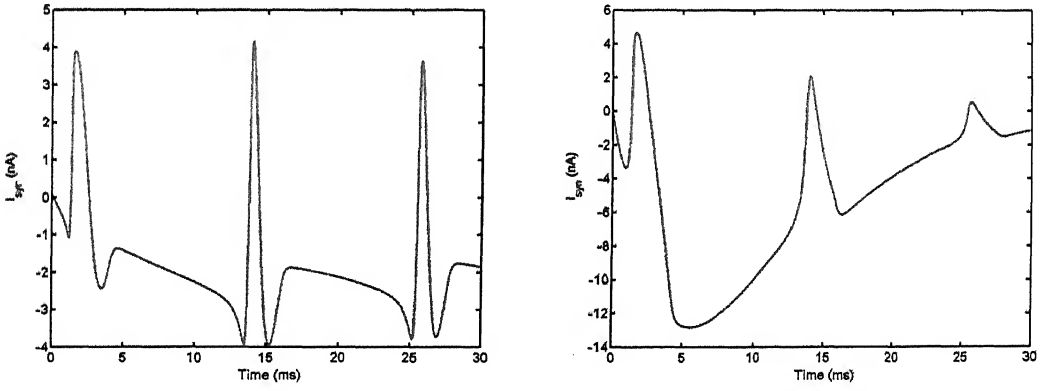

(a) Synapse A (b) Synapse B

Figure 3.7: Synaptic inputs to Dendrites

A nerve cell generally has a huge number of dendrites. It is not necessary that a neuron receives signal only from one synapse. In order to maintain the generality, two synapses have been considered that pose different characteristics. The topology of the dendrites are given in Table 3.2.

The responses of *Dendrite A* and *Dendrite B* are shown in Figure 3.8. The response of *Dendrite A* is very much different from Figure 3.1. Two factors are involved for

Table 3.2: Topology of different dendrites

Part	Input	Length	Diameter near synapse	Diameter near soma
Dendrite A	Synapse A	1.0 mm	12 μm	16 μm
Dendrite B	Synapse A	1.2 mm	8 μm	13 μm
Dendrite C	Synapse B	0.8 mm	10 μm	12 μm

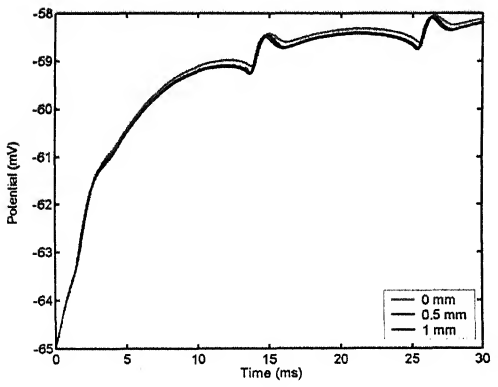

(a) Dendrite A

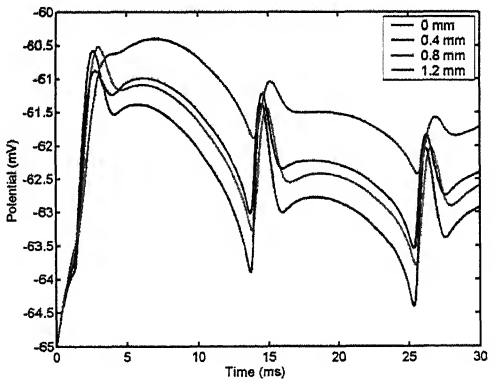

(b) Dendrite B

Figure 3.8: Potential propagation in Dendrite A and Dendrite B

the change in response of the dendrite – the synaptic current and the time constant. Synaptic current is not exactly pulse shaped as considered in earlier case and also repetitive. Moreover, the time constant of the passive membrane is much larger than that of the synaptic current. This does not allow the dendritic potential to fall much. Also, there is no significant attenuation in the potential as it propagates. The synaptic current is negative for a larger time instant. It is distributed along the length of the dendrite instead of the injection only at its terminal. The result is almost similar potential waveform irrespective of space.

Response of *Dendrite B* shows a clear rising and falling edge. The synaptic current distribution along its length is somewhat different from that of *Dendrite A*. The time constant is also lesser in case of *Dendrite B*. The attenuation or growth in potential with respect to space is more significant. The reason for growth in potential is same with earlier case. Waveshape of potential propagation in *Dendrite A* and *Dendrite B* are similar with the difference only in rising and falling time.

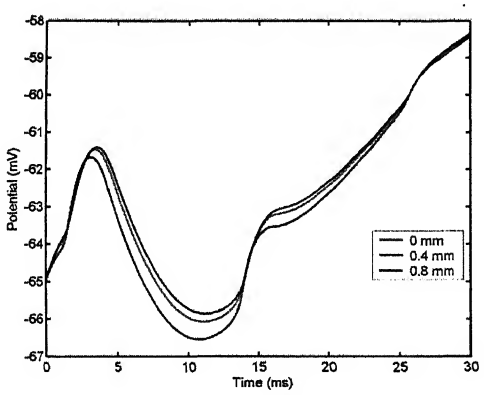

Figure 3.9: Potential propagation in Dendrite C

Dendrite C receives the signal from *Synapse B* which is *NMDA* synapse. The response is shown in Figure 3.9. The potential near soma falls below the resting potential when the time is 8.14 ms. It remains negative with respect to the resting value up to $t = 13.96$ ms. This is due to the high inhibitory synaptic current between 2.6 ms to 13.8 ms.

3.5.3 Soma

The signals from dendrites reach to soma as a form of potential. The absolute magnitudes of these potentials are negative with respect to zero reference voltage. However, the effective magnitudes *i.e.* the magnitudes with respect to the resting potential may be positive or negative. The effective potential near soma for i^{th} dendrite is given by,

$$VD_i^{effective} = VD_i^{absolute} - V_{Rest}$$

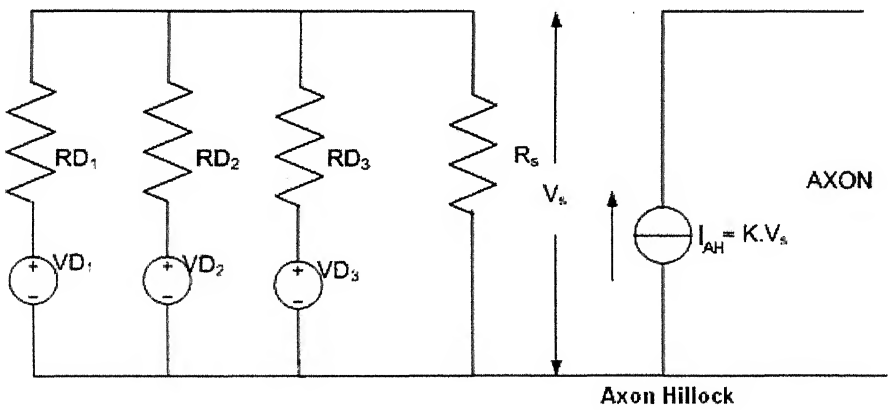

Figure 3.10: The model of soma

A schematic diagram showing the soma model is given in Figure 3.10. The voltage sources VD_1, VD_2 and VD_3 are the effective potentials of *Dendrite A*, *Dendrite B* and *Dendrite C* respectively near soma. RD_1, RD_2 and RD_3 are the corresponding

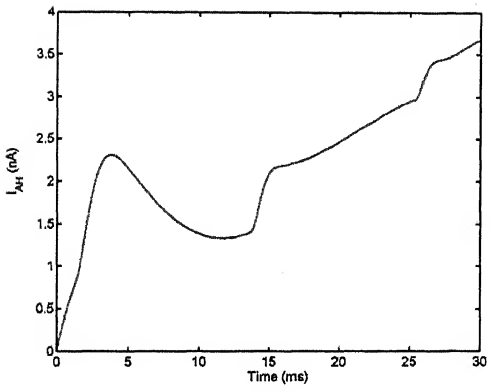

Figure 3.11: Current injection at axon hillock

resistances through which the dendrites are connected to soma. The summed potential V_S at soma appears across the resistance R_S. The soma acts as a buffer circuit that not only sums up the dendritic potentials and passes through the axon but also isolates the axon from dendrites. The current at *Axon hillock* generates the action potential. This current shown by KV_S is generated due to the multiplication of summed potential V_S with the conductance that connects soma with *Axon hillock*. The current at *Axon hillock* is computed by carrying out the nodal analysis. This current is given by Equation 3.13

$$I_{AH} = K\frac{\frac{VD_1}{RD_1} + \frac{VD_2}{RD_2} + \frac{VD_3}{RD_3}}{\frac{1}{RD_1} + \frac{1}{RD_2} + \frac{1}{RD_3} + \frac{1}{R_S}} \tag{3.13}$$

where K is a constant that depends on conducatnce between soma and *Axon hillock*. The time course of this current is plotted in Figure 3.11. The magnitude of the current increases with the time from 0 ms to 3.7 ms. Then its starts decreasing up to 11.8 ms as the effective potential of *Dendrite C* is negative for this time span. The effect of this current on the generation of action potential is discussed in the next section.

3.5.4 Axon

The axon considered for the analysis has a length of 12 cm with it diameter tapers from 8 μm near soma to 2 μm at its end near synapse. The axon has no branches spreading out of it. Multicompartmental method is used for modeling the axon. Response is shown in Figure 3.12. It has been found earlier that there was no initiation of spike in case of continuous current injection until the current magnitude exceeds 10 nA. In this case, the maximum magnitude of the current reaches 3.7 nA within the analysis time span. The topology of axon is also same in this case as in earlier case. However, the action potential is generated and propagated for the complete neuron model. The delay is also reduced. For the first spike, there is almost no delay when it propagates from 4 cm to 12 cm. The only change is in the shape of injected current. Therefore it can be concluded that the action potential may be generated for a lesser intensity of current if its magnitude is rising with respect to time. The action potential that arrives at the synapse is allowed to participate in the synaptic activities in order to compare it with earlier synaptic response.

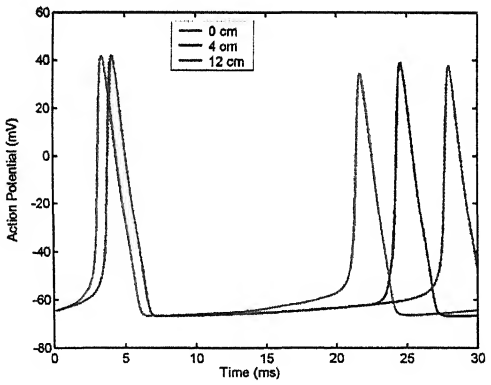

Figure 3.12: Response of axon in complete neuron model

The responses for the synapses are shown in Figure 3.13. As mentioned earlier, two cases have been considered. Part(a) of the figure shows the response when the axon is terminated at *Non-NMDA Synapse* and Part(b) shows the same when it terminates at *NMDA Synapse*. The characteristics are found to be almost similar except the frequency of occurrence of the synaptic current.

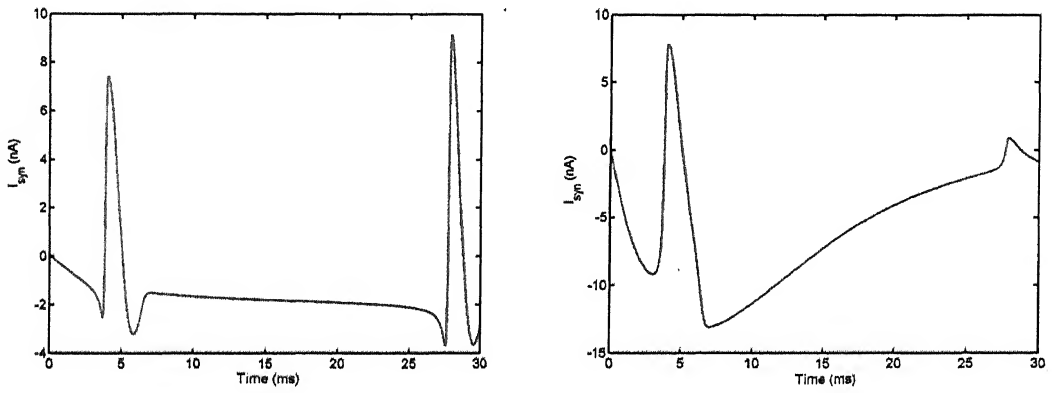

(a) Synapse C (b) Synapse D

Figure 3.13: Synaptic current

A three dimensional plot for the potential distribution with respect to time and space for the three dendrites and axon are shown in Figure 3.14.

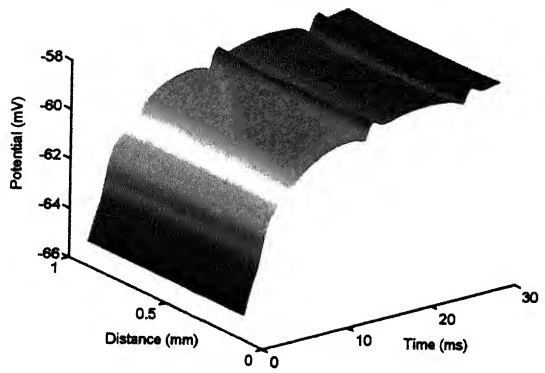

(a) Dendrite A

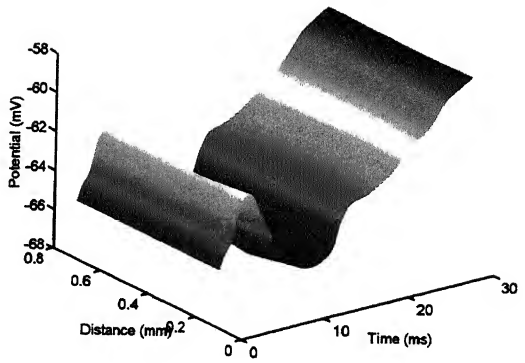

(b) Dendrite B

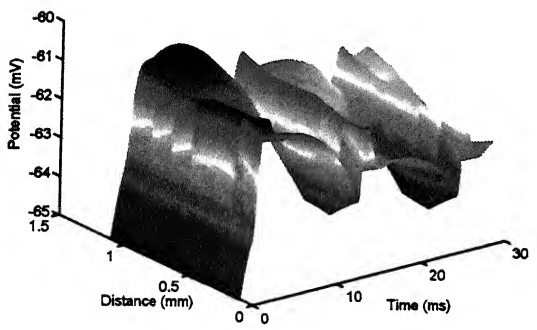

(a) Dendrite C

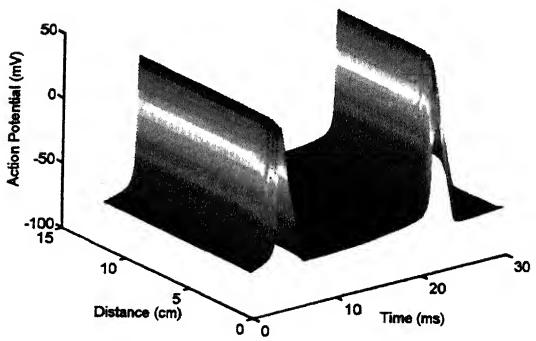

(b) Axon

Figure 3.14: Three dimensional plot for potential distribution in dendrites and axon

3.6 Summary and Conclusion

In this chapter, the behavior of neuron is analyzed when the signal propagates in it. The cable theory has been used to model the dendrites and axon. The graded potential propagation in a passive dendritic tree under constant current stimulation is analyzed. It has been considered that the stimulus is not only applied to its end, rather it is distributed at its extensions near the synapse. The effect of stimulus with constant magnitude is also studied to model the active membrane of the axon. The study includes the effect of noise. A new method based on *Fourier Series* is proposed to model the axon. Finally the behavior of the complete realistic neuron model has been investigated.

It has been found that the behavior of propagating signal is highly dependent upon the nature of membrane. There is no initiation of spike in case of passive membrane. The passive membrane not only introduce the delay in signal, but also attenuation. On the other hand, there is occurrence of spike when signal propagates in active membrane. Although a delay occurs depending upon its speed, there is no attenuation observed. For the considered topology of axon, a steady current of magnitude 11 nA initiate action potential. A lower value of current magnitude may also result in spiking if noise is induced. However, the model of axon is very robust or in other words immune to noise as a noise with 5 dBW power is also almost incapable to generate action potential when the current is 9 nA. The initiation of action potential also depends on the shape of the stimulus waveform. The *Fourier Series* method may be used to avoid the complexity of multicompartmental model for approximated work. The complete neuron modeling provides the details of information processing in neuron. The waveform of *Synapse A* is identical with that of *Synapse C* . Similarly, the waveforms of *Synapse B* and *Synapse D* are identical. The difference is only in the magnitudes and in time of occurring of current pulses. The *Synapse A* and *Synapse B* considers the dynamics of a point neuron HH model as a presynaptic potential and hence is the difference. The identical response of the synapses cross checks the validation of the model.

Chapter 4

Conclusion

4.1 Work Done

The neurons are coupled together to work synchronously for performing a specific task. In this work, the effect of coupling strengths on the network of neurons is studied and the following conclusions are drawn –

- The weakly coupled neurons are not in synchronism as the coupling current that being proportional to potential difference between the neurons, controls the synchronous behavior of the neurons, is less.
- The coupled neurons are in complete synchronism for strongly coupled system and there is no phase difference between successive firing of the neurons.
- The variation in coupling strength results in different firing frequency of both the neurons. The firing frequency is more in case of strongly coupled system compared to weakly coupled system.
- Synchronization phenomenon and variation in excitability is depicted by plotting bifurcation diagram for the pair of coupled neurons.

A similar analysis has also been carried out for the interconnections of three neurons and the following observations are made according to simulation results.

- In case of weakly coupled system, all the three neurons show spiking behavior whereas a neuron was uncapable to cross the subthreshold regime when not coupled with the other two neurons. The coupling mechanism provides additional stimulus which brings the neuron to oscillatory from stable state.

- Similar to two coupled neuron case, the three strongly coupled neurons fire synchronously.

- Bifurcation analysis is carried out on coupled system and it is found that for weakly coupled system with variation in bifurcation parameter, the neurons enter into oscillatory state earlier as compared to strongly coupled system.

In Chapter 3, signal propagation in neuron structure is studied and different approach for investigating the signal propagation is presented. The following conclusions are drawn from this analysis.

- The addition of white gaussian noise reflects the biophysical activities such as ephaptic interaction and uneven opening and closing of ion channels and this facilitates in signal transmission by slightly reducing the threshold. Thus noise helps in firing, but not in great extent.

- A Fourier series based methodology for signal propagation in neuron is proposed. This reduces the computational complexity.

- In last section of this chapter, an overall signal propagation in a neuron structure by considering the dynamics of all the components are presented. It is found that the current at *Axon hillock* is not steady and variation in current at *Axon hillock* results in variation in spike speed.

4.2 Future Scope

- The behavioral analysis on the coupled neuron model can be extended to find out the existence and effect of *Chaos* for a large population of neurons.
- Study can be carried out on the synchronization of nonlinearly coupled neurons.
- In the complete neuron model, the dendrites are assumed to be located very closely and therefore the resistance between two dendrites are ignored. The study of this model with the inclusion of these resistances may capture some new characteristics.
- The effect of dendritic spines on the response of complete neuron can also be investigated.
- As the dynamics of a complete neuron model is revealed in this thesis work, the analysis can be carried out on a population of neurons.

References

[1] Arvanitaki, A. "Effects Evoked in an Axon by the Activity of a Contiguous One", Neurophysiol J., 5, 89-108, 1942.

[2] Baier, G. and Muller, M. "Excitable Chaos in Diffusively Coupled FitzHugh-Nagumo Equations", Revista Mexicana De Fisica, 50, 5, 422-426, 2004.

[3] Bezrukov, S. M. and Kish, L. B. "How Much Power Does Neural Signal Propagation Need?", Smart Materials and Structures, 11, 800-803, 2002.

[4] Breakspear, M., Terry, J. R. and Friston, K. J. "Modulation of Excitatory Synaptic Coupling Facilitates Synchronization And Complex Dynamics in a Biophysical Model of Neuronal Dynamics", Network: Computation in Neural Systems, 14, 703-732, 2003.

[5] Brown, D., Feng, J. and Feerick, S. "Variability of Firing of Hodgkin-Huxley And FitzHugh-Nagumo Neurons with Stochastic Synaptic Input", Physical Review Letters, 82, 23, 4731-4734, 1999.

[6] Chklovskii, D. B. and Stepanyants, A. "Power-Law for Axon Diameters at Branch Point", BMC Neuroscience, 4:18, 2003.

[7] Clark, J. W. and Plonsy, R. "Fiber Interaction in a Nerve Trunk", Biophysics J., 11, 281-294, 1971.

[8] Coombes, S. "From Periodic Travelling Waves to Travelling Fronts in the Spike-Diffuse-Spike Model of Dendritic Waves", Mathematical Biosciences J., 170, 155-172, 2001.

[9] Dayan, P. and Abbott L. F. "Theoretical Neuroscience", The MIT Press, Cambridge, 2001.

[10] Elson, R. C., Selverston, A. I., Huerta, R., Rulkov, N. F., Rabinovich, N. I. and Abarbanel, H. D. I. "Synchronous Behavior of Two Coupled Biological Neurons", Physical Review Letters, 81, 25, 5692-5695, 1998.

[11] Feng J. and Li, G. "Neuronal Models with Current Inputs", J. Phys., 24, 16491664, 2001.

[12] FitzHugh, R. "Mathematical Models for Excitation And Propagation in Nerve", Biological Engineering. H.P. Schawn (Ed.), New York: McGraw-Hill, 1969.

[13] Gao, Y. "Chaos And Bifurcation on Space Clamped FitzHugh-Nagumo System", Academy of Mathematics and System Sciences, Chaos Solutions and Fractals, 943-956, 2004.

[14] Gerloff, C., Richard, J., Hadley, J., Schulman, A. E., Honda, M. and Hallett, M. "Functional Coupling and Regional Activation of Human Cortical Motor Areas during Simple, Internally Paced And Externally Paced Finger Movements", Brain, 121, 1513-1531, 1998.

[15] Gordon, H. T. and Welsh, J. H. "The Role of Ions in Axon Surface Reactions to Toxic Organic Compounds", Journal of Cellular and Comparative Physiology, 31, 3, 395-419, 2005.

[16] Hausser, M., Stuart, G., Racca, C. and Sakmann, B. "Axonal Initiation And Active Dendritic Propagation of Action Potential in Substantial Nigra Neurons", Neuron J., 15, 637-647, 1995.

[17] Hodgkin, A. and Huxley, A. "A Quantitative Description of Membrane Current And Its Application to Conduction And Excitation in Nerve", J.Phisiol. (Lond.), 117, 500-544, 1952.

[18] Holt, G. R. "A Critical Reexamination of Some Assumptions And Implications of Cable Theory in Neurobiology", Doctoral dissertation, California Institute of Technology, 1998.

[19] Jing, Z., Chang, Y. and Guo B. "Bifurcation And Chaos in Discrete FitzHugh-Nagumo System", Chaos Solutions and Fractals, 21, 3, 701-720, 2004.

[20] Kandel, E. R. "Nerve Cells And Behavior", In Eric R. Kandel, James H. Schwartz, and Thomas M. Jessell, eds. Principles of Neural Science, 3rd ed. Elsevier, NY, 1991.

[21] Kavasseri, R. G. "Bifurcations in a Synaptically Coupled Morris-Lecar Neuron Model", Proc. Hawaii International Conference on Sciences Honolulu, Hawaii, 2004.

[22] Koch, C. "Biophysics of Computation: Information Processing in Single Neurons", Oxford University Press, 1999.

[23] Lord G. J. and Coombes, S. "Traveling Waves in the Baer And Rinzel Model of Spine Studded Dendritic Tissue", Physica D., 161, 1-20, 2002.

[24] Mishra, D., Yadav, A. and Kalra, P. K. "Chaotic Behavior in Neural Networks and FitzHugh-Nagumo Neuronal Model, Proceedings of ICONIP-2004, India, LNCS 3316, 868-873, 2004.

[25] Morris, C. and Lecar, H. "Voltage Oscillations in the Barnacle Giant Muscle Fiber", Biophysics J., 35, 193-213, 1981.

[26] Muratov, C. B. "A Quantitative Approximation Scheme for the Traveling Wave Solutions in the HodgkinHuxley Model", Biophysical J., 79, 2893-2901, 2000.

[27] Nagumo, J. S., Arimoto, S., and Yoshizawa, S. "An Active Pulse Transmission Like Simulating Nerve Axon", Proceedings of the IRE, 50, 2061-2074, 1962.

[28] Penn, A. A., Wong, R. O. and Shatz, C. J. "Neuronal Coupling in the Developing Mammalian Retina", Neuroscience J, 14, 3805-3815, 1994.

[29] Perkel, D. H. and Mulloni, B. "Electronics Properties of Meurons: Steady-State Compartmental Models", Neurophysiol J., 41, 621-639, 1998.

[30] Pinto, R. D.,Verona, P., Volkovskii, A., Abarbanel H. D. I and Rabinovich, M. I. "Synchronous Behavior of two Coupled Electronic Neurons", Physical Review E., 62, 2644-2655, 2000.

[31] Purves, D., Augustine, G. J., Fitzpatrick, D., Katz, L. C., LaMantia, A. S., McNamara, J. O., Williams, S. M. "Neuroscience", Sinauer Associates, Inc., MA, 2001.

[32] Reinker, S., Puil, E. and Miura, R. M. "Resonances And Noise in a Stochastic Hindmarsh-Rose Model of Thalamic Neurons", Bulletin of Mathematical Biology, 65, 641-663, 2003.

[33] Rinzel, J. "A Formal Classification of Bursting Mechanisms in Excitable Systems", In Mathematical Topics in Population Biology, Morphogenesis and Neurosciences, Lecture Notes in Biomathematics, Springer-Verlag, NY, 71, 267-281, 1987.

[34] Rinzel, J. and Ermentrout, G. B. "Analysis of Neural Excitability And Oscillations", Methods in Neuronal Modeling, MIT Press, Cambridge, MA, 1989.

[35] Rinzel, J. and Ermentrout, B. B. "A Formal Classification of Bursting Mechanism in Excitable Systems", In Koch, C., & Segev, I (Eds.) Methods in neuronal modeling. Cambridge: The MIT Press, 1998.

[36] Schalkoff, R. J. "Artifical Neural Networks", The McGraw-Hill Companies, Inc., NY, 1997.

[37] Stacey, W. C. and Durand, D. M. "Stochastic Resonance Improves Signal Detection in Hippocampal CA1 Neurons", Neurophysiol J., 83, 1394-1402, 2002.

[38] Strogatz, S. H. "Nonlinear Dynamics And Chaos", Persus Books Publishing, LLC, 1994.

[39] Suslov, S. K. "An Introduction to Basic Fourier Series, Developments in Mathematics", Vol. 9, Kluwer Academic Publishers, 2003.

[40] Terakawa, S. "Periodic Responses in Squid Axon Membrane Exposed Intracellularly And Extracellularly to Solutions Containing a Single Species of Salt", Journal of Membrane Biology, 63(1-2):51-9, 1981.

[41] Tuckwell, H. and Rodrigueguez, R. "Analytical and Simulation Results for Stochastic FitzHugh-Nagumo Neurons And Neural Networks", Journal of Computational Neuroscience, 5, 91-113, 1998.

[42] Ucar, A., Lonngren, K. E. and Bai, E. W. "Synchronization of the Coupled FitzHugh-Nagumo Systems", Chaos, Solutions and Fractals, 20, 1085-1090, 2004.

[43] West, R. M. E. "On the Development and Interpretation of Parameter Manifolds for Biophysically Robust Compartmental Models of CA3 Hippocampal Neurons", University of Minnesota Dissertation, 1996.

[44] Widrow, B. and Steams, S. "Adaptive Signal Processing", Prentice-Hall, Englewood Cliffs, NJ, 1985.

[45] Zak, S. H. "Systems And Control", Oxford University Press, Inc., NY, 2003.

[46] http://faculty.washington.edu/chudler/introb.html

[47] http://inside.salve.edu

[48] http://www.biologydaily.com

List of Publications

Journals

1. Yadav, A, Mishra, D., **Ray, S.**, Yadav, R.N. and Kalra, P.K. "Functional Mapping with Single Integrate-and-Fire Neuron", International Journal of Computational Intelligence (IJCI), 2005. (Accepted)

Conferences

1. **Ray, S.**, Mishra, D., Yadav, A. and Kalra, P.K. "Propagation of Action Potential and Concept of Ephaptic Interaction in Axon", International Conference on Cognitive Science, Allahabad, 182-187, 2004.

2. **Ray, S.**, Mishra, D., Yadav, A. and Kalra, P.K. "From Point Neuron to Axon Modeling: A New Approach", International Conference on Neural Information Processing, ICONIP–2005, 2005. (Submitted)

3. Mishra, D., Yadav, A., **Ray, S.** and Kalra, P.K. "Some Aspects of the Dynamical Analysis of Integrate And Fire Neuron Model And Synaptic Interaction", National Conference on Recent Advances in Power, Signal Processing And Control, Rourkela, 174-179, 2004.

4. Mishra, D., Yadav, A., **Ray, S.** and Kalra, P.K. "Effects of Noise on the Dynamics of Biological Neuron Models", Proceedings of the Fourth IEEE International Workshop WSTST05, Muroran, 61-69, 2005.

5. Mishra, D., Yadav, A., **Ray, S.** and Kalra, P.K. "Nonlinear Dynamical Analysis of Single Neuron Models and Study of Chaos in Brain", International Conference on Cognitive Science, Allahabad, 188-193, 2004.

6. Mishra, D., Yadav, A., **Ray, S.** and Kalra, P.K. "The Effect of Synaptic Bombardment in Dynamics of Biological Neuron Models", International Conference on Cognitive Science, Allahabad, 200-205, 2004.

7. Mishra, D., Yadav, A., **Ray, S.** and Kalra, P.K. "Nonlinear Dynamical Analysis on Coupled Modified FitzHugh-Nagumo Neuron Model", Proceedings of International Symposium of Neural Network, Chongqing, 2005. (Accepted)

8. Mishra, D., Yadav, A., **Ray, S.** and Kalra, P.K. "Bifurcation Analysis in Modified FitzHugh-Nagumo Neuronal Model", National Conference on Control And Dynamical Systems,Bombay, 2004. (Accepted)

Appendix A: Implicit Integration Method

The numerical solution of multicompartment model requires the value of potential at a later time stage. This requires implicit integration method. Two types of implicit integration method are widely used–*Crank-Nicholson method* and *Backward Euler method.* The membrane potential for the μ^{th} compartment is given by

$$C\frac{dV_m^\mu(t)}{dt} = -i_m^\mu(t) + g^{\mu,\mu-1}\left(V_m^{\mu-1}(t) - V_m^\mu(t)\right) + g^{\mu,\mu+1}\left(V_m^{\mu+1}(t) - V_m^\mu(t)\right) + I_{inj}^\mu(t)$$

This equation can be written as

$$\frac{dV_m^\mu(t)}{dt} = A^\mu V_m^{\mu-1} + B^\mu V_m^\mu + C^\mu V_m^{\mu+1} + D^\mu$$

where

$$A^\mu = g^{\mu,\mu-1}/C; \quad B^\mu = \left(g^{\mu,\mu-1} + \sum_i g_i^\mu + g^{\mu,\mu+1}\right)/C$$

$$C^\mu = g^{\mu,\mu+1}/C; \quad D^\mu = \left(g_i^\mu E_i + I_{inj}^\mu\right)/C$$

This generates a set of coupled differential equations. For $z \in [-1,\ 1]$

$$V_m^\mu(t + z\Delta t) \approx V_m^\mu(t) + z\Delta V_m^\mu$$

The finite difference method yields,

$$\Delta V_m^\mu(t) = \left(A^\mu V_m^{\mu-1}(t + z\Delta t) + B^\mu V_m^\mu(t + z\Delta t) + C^\mu V_m^{\mu+1}(t + z\Delta t) + D^\mu\right)\Delta t$$

Approximating,

$$\Delta V_m^\mu = a^\mu V_m^{\mu-1} + b^\mu V_m^\mu + c^\mu V_m^{\mu+1} + d^\mu$$

where

$$a^\mu = A^\mu z\Delta t; \quad b^\mu = B^\mu z\Delta t; \quad c^\mu = C^\mu z\Delta t$$

$$d^\mu = \left(D^\mu + A^\mu V_m^{\mu-1}(t) + B^\mu V_m^\mu(t) + C^\mu V_m^{\mu+1}(t)\right)\Delta t$$

For N compartment model, $a^1 = 0$ and $c^N = 0$. The potential change for the $(\mu - 1)^{th}$ compartment is given by,

$$\Delta V_m^{\mu-1} = \frac{c^{\mu-1}\Delta V_m^{\mu} + d_{new}^{\mu-1}}{1 - b_{new}^{\mu-1}}$$

where,

$$b_{new}^{\mu+1} = b^{\mu+1} + \frac{a^{\mu+1}c^{\mu}}{1 - b_{new}^{\mu}}; \qquad b_{new}^{1} = b^{1}$$

$$d_{new}^{\mu+1} = d^{\mu+1} + \frac{a^{\mu+1}d_{new}^{\mu}}{1 - b_{new}^{\mu}}; \qquad d_{new}^{1} = d^{1}$$

At the end of the cable,

$$\Delta V_m^N = \frac{d_{new}^N}{1 - b_{new}^N}$$

The algorithm for solving the multicompartment model is: compute b_{new}^{μ} and d_{new}^{μ} down the length of the cable, then solve for ΔV_m^N and iterate back up the cable. This process takes $2N$ steps.

For *Crank-Nicholson method,* $z = 0.5$ and for *Backward Euler method,* $z = 1.0$. The *Backward Euler method* is more stable whereas the *Crank-Nicholson method* gives more accurate result.